Nonlinear Dynamics and Interactions in Power Electronic Systems

Mohammed Al-Fayyoumi

Thesis submitted to the Faculty of the

Virginia Polytechnic Institute and State University

in partial fulfillment of the requirements for the degree of

Master of Science

in

Electrical Engineering

Ali H. Nayfeh, Chair

Dusan Borojevic

Hugh Van Landingham

December 1, 1998

Blacksburg, Virginia

Nonlinear Dynamics and Interactions in Power Electronic Systems

Mohammed Al-Fayyoumi

(ABSTRACT)

The nonlinear dynamics of PWM DC-DC switching regulators operating in the continuous conduction mode are investigated. A quick review of the existing analysis techniques and their limitations is first presented. A discrete nonlinear time-domain model is derived for open-loop DC-DC converters. This model is then extended for closed-loop regulator systems implementing any type of compensation scheme. The equilibrium solutions of the closed-loop system are calculated and their stability is determined. The methods developed are used to study the dynamic behavior of a DC-DC buck regulator implementing different types of compensation design: proportional, integral, proportional-integral, and proportional-integral-derivative feedback control. A detailed bifurcation analysis of the dynamic solutions as a design or a control parameter is changed is presented. A period-doubling route to chaos is shown to exist in voltage-mode regulators, depending on the values of the parameters of the compensator and the input voltage. An investigation of the behavior of the converter in the instability regions has been carried out to shed light on its bifurcations. The interactions of input filters with DC-DC switching-mode regulators are investigated as well. It is shown that the small-signal averaged model widely used in the design of DC-DC regulators does not provide a complete understanding of the stability of the filter-regulator

system. It can only provide the local borders of small-signal stable operation. The large-signal time-domain nonlinear averaged model is used to further understand the interaction on the slow scale using nonlinear analysis techniques. No fast scale interactions, however, can be predicted using this model. A complete nonlinear switching model is thus used to investigate the interaction of the filter and the regulator on all scales: fast and slow.

To my parents with love and gratitude

Acknowledgments

I am deeply indebted to Dr. Ali Nayfeh who have given freely of his time, knowledge and resources to advise, guide, and support me since day one. This work would have not been possible without him. I also wish to acknowledge and thank Dr. Dusan Borojevic for his advice and support throughout all the stages of this work. I am also grateful to Dr. Hugh Van Landingham for accepting to serve as a member of my committee.

Particular acknowledgments go to all the people of the nonlinear dynamics laboratory at Virginia Tech. Their continuous encouragement and valuable comments were greatly appreciated.

Special thanks go to my family, whom I was blessed to have their love and support all these years. It is mainly from them I got the strength and inspiration that enabled me to finish this work and to them goes a great part of my gratitude.

Thanks to the Office of Naval Research for providing the financial support under Grant No. N00014-96-1-1123.

Finally, most sincere gratitude are due to God, the most graceful, the most merciful.

Contents

List of Figures

Chapter 1

Introduction

Switching-mode DC-DC regulators are nonlinear systems that represent different circuit topologies or configurations within one switching cycle. For the continuous conduction mode, there are two topologies. For the discontinuous conduction mode of operation, a third configuration has to be added to yield a total of three topologies. In each configuration, the system can be described by linear state equations. However, for a complete switching cycle, the system becomes piecewise linear. Switching between the different networks will vary from cycle to cycle depending on the output of the system, and this further complicates the analysis.

The static conversion properties of the elementary switching converters (buck, boost, and buck-boost) have been thoroughly understood since the early 1950s and well-known since the 1970s. This is one of the main reasons of their ever-increasing number of applications in electrical energy conversion. However, the complete dynamic behavior of switching regulators still have to be further understood and improved. This is not possible without an in-depth understanding of the operation of such circuits and without easy-to-use and accurate models.

Modeling and analysis of switching DC-DC regulators can be either numerical or analytical. In numerical techniques, various algorithms or circuit simulators are used to produce quantitative results. These methods are easy to use. They posses accuracy and universality and they are applicable when no equivalent model is available. However, they are time-consuming and fail to provide the design insight needed to understand the behavior of switching regulators. Analytic techniques, on the other hand, provide analytic expressions representing the operation of DC-DC converters, hence enabling qualitative understanding of the operation and performance of the converters.

To date, most analytic techniques of modeling and analysis of DC-DC switching regulators implement different degrees of approximations and varying levels of restrictions in order to fit them into the framework of conventional linear system theory where there is a large body of standard theory for the analysis and design of linear feedback systems. In general, modeling techniques can be (a) continuous, (b) discrete, or (c) combination of continuous and discrete models.

Perhaps the most popular continuous technique is the small-signal analysis, which uses either circuit averaging (Wester and Middlebrook, 1972), state-space averaging (Middlebrook and Cuk, 1977; Cuk and Middlebrook, 1977), or PWM switch model (Vorperian, 1990a,b). Middlebrook and Wester (1972) developed analytical techniques to represent buck, boost, and buck-boost converters by approximate continuous models. Simple analytical expressions in terms of the circuit components were derived to characterize the low-frequency response of such systems. Middlebrook and Cuk (1977) generalized the above technique by introducing the state-space averaging method. They replaced the state-space descriptions of the switched networks by a single state-space description, hence eliminating the switching process from consideration and representing the average effect of the switched networks in one cycle of operation. By means of state-space averaging, the original nonlinear discrete system was simplified into a continuous system. This system was further simplified by perturbing the averaged system and then linearizing the resulting perturbed equations around the steady-state values. After a considerable amount of matrix manipulations, the system characteristics such as input impedance, output impedance, line-to-output transfer function, and control-to-output characteristics, were obtained. Vorperian (1990a,b) presented a circuit-oriented approach to the analysis of PWM converters. His method relied on the identification of a three-terminal nonlinear device, called the PWM switch, which consists of the active and passive switches in a PWM converter. Once the invariant properties of the PWM switch were determined, an average equivalent circuit model was derived, and DC and small-signal characteristics of the converter were obtained by a simple substitution of the PWM switch with its equivalent circuit model.

Continuous techniques make certain assumptions in order to achieve the final simplified averaged model. The first simplifying assumption is the linear ripple approximation or the straight line approximation, which approximates the matrix exponentials appearing in the solutions of linear systems by the first two terms of their Taylor series expansions. This approximation is valid when the natural frequencies of the converter are all well below the switching frequency such that the solutions are approximately linear. This is the case for a well-designed PWM converter. The second approximation is in effect averaging the output or the duty ratio function, and is less justified. Note that, in a closed-loop regulator system, the output is responsible for generating the duty ratio function. This approximation effectively eliminates a sampler, and hence may be expected to affect the accuracy of the averaging methods at frequencies approaching one-half the switching frequency, known as the high frequency regime or the fast-scale dynamics.

Although averaged models have been employed successfully in many applications, they fail to predict the fast-scale dynamics due to the switching behavior of the regulator; they can only capture the slow-scale dynamics. The accuracy of these models degrades as the modulation frequency approaches one-half the switching frequency. They fail to predict the instability occuring in current-mode converters.

Exact discrete modeling techniques (Prajoux, Marpinard, and Jalade, 1976; Capel, Ferrante, and Prajoux, 1975; Lee, Iwens, and Yu , 1979) make no simplifying assumptions as those made by the averaging techniques. The switched continuous system is replaced by a discrete system that describes the state of the system at the switching frequency. Hence, these modeling techniques can predict the fast-scale dynamics. Prajoux, Marpinard, and Jalade (1976) presented a discrete approach, which is capable of accurately describing a system with varying structures within a given period by a linearized discrete time-domain model. It was applied to modeling a boost converter operating in the continuous conduction mode. Capel, Ferrante, and Prajoux (1975) applied this method to multi-loop buck and boost regulators in both types of conduction modes. Lee, Iwens, and Yu (1979) extended this analysis to the three types of converters: buck, boost, and buck boost.

Because of the complexity of the switching models, more simplified techniques that combine both continuous and discrete models were developed (Brown and Middlebrook, 1981; Shortt and Lee, 1983; Ridley, 1991). Brown and Middlebrook (1981) developed a new modeling approach combining continuous and discrete techniques. Their model did not treat the duty ratio as a smooth, slowly time-varying wave, but as a waveform of discrete pulses. The power stage model was still based on the averaging techniques. Shortt and Lee (1983), on the other hand, developed a discrete-averaged model by combining the aforementioned averaging and discrete techniques. The model used the averaged state-space form of the averaging technique and determined the output by a discrete sample. Ridley (1991) presented a new small-signal model for pulse-width-modulated converters operating with current-mode control. Sampled-data modeling was applied to the current-mode cell, which is common to all converters, and the results obtained were simplified to give a model for analysis and design. As these hybrid methods include the effects of the sampling action caused by the switching in one way or another, they succeed where averaged models fail in predicting the boundaries of fast-scale instabilities.

Recently, DC-DC switching regulators were observed to behave in a chaotic manner. More interesting nonlinear behaviors, such as subharmonics and a period-doubling route to chaos, were also encountered. To explore these interesting phenomena, one needs discrete models. Chaos and subharmonic instability in DC-DC converters were observed and described by Brockett and Wood (1984), Wood (1989), Jefferies, Deane, and Johnstone (1989), Deane and Hamill (1990), Deane (1992), Hamill, Deane, and Jefferies (1992), and Fossas and Olivar (1996). Their works illustrate how chaos can occur in simple voltage-mode PWM DC-DC buck converters operating in the continuous conduction mode.

Chaos was also studied for a current-programmed boost PWM DC-DC switching converter operating in the continuous conduction mode by Hamill and Jefferies (1988), Krein and Bass (1989, 1990), Zafrany and Ben-Yaakov (1995), Chan and Tse (1996a,b), Marrero, Font, and Verghese (1996), and in the discontinuous conduction mode by Tse and Adams (1990) and Tse (1994a,b).

In the aforementioned studies, the analyses were limited to a specific type of converters and feedback design. Limited physical insight was provided as well. The modeling technique described in this thesis is nonlinear, exact, and applicable to any type of converter implementing any type of controller, including the error amplifier design and the duty-ratio controller. This technique will enable the examination of the behavior of the regulator system in all regions: stable and unstable. It also allows the prediction of the subharmonic behavior and the exploration of chaos within the regions of instability.

In Chapter 2, we derive a complete discrete-time model for nonlinear DC-DC converters operating in the continuous conduction mode. This model provides the discrete state-space description of the converter, the equilibrium solutions, and their stability through eigenvalue analysis. The model can be applied independently from (1) the topology of the converter, (2) its operating mode, and (3) the nature of the controlled variable. The model yields a truly general method for analyzing power regulators. It is easy to modify this model for different kind of switching regulators and extend it for larger or more complicated systems

In Chapter 3, we compare different examples of a DC-DC buck converter implementing different compensation schemes. Moreover, we compare the results obtained using the exact modeling technique with those obtained using the averaging technique.

In chapter 4, we address a classical stability problem resulting when integrating subsystems, the subsystem interaction problem. System instability and performance degradation can result from interaction between subsystems. Even though each subsystem may be well-designed for stand-alone operation, interaction can lead to stability and performance problems after system integration. When connected to a switching regulator, an input filter can cause system instability and performance degradation due to the interaction with the regulator. Filter-regulator interaction on the slow scale or the averaged behavior was studied by Yu and Biess (1971), Middlebrook (1976, 1978), and Lee and Yu (1979). Necessary conditions for system stability on the slow scale were determined and guidelines for designing the input filter with minimal degradation were identified. This small-signal averaged analysis is, however, not complete owing to two reasons. First, on the slow scale, it neglects the nonlinear effects and hence overlooks subcritical instabilities, which in turn lead to a wrong conclusion about the borders of stability. Second, the small-signal averaged analysis neglects the interaction on the fast scale. As shown in this thesis, although the system might be stable to slow-scale disturbances, it might be unstable to fast-scale disturbances. In this thesis, these two aspects neglected by previous interaction studies are investigated.

In chapter 5, we present the conclusions and recommendations.

Chapter 2

Modeling

Switched-mode DC-DC regulators consist, in general, of three basic functional blocks: power stage, error processor, and modulator or duty-ratio controller. The power stage or power convertor, illustrated in Fig. 2.1, can be one of three basic configurations: buck, boost, or buck-boost. The error amplifier is the feedback compensation network. It compares the output voltage with a reference signal and the generated control signal is then used to activate the modulator. The modulator includes a ramp generator, a comparator, and a driver in order to achieve duty-ratio control of the power switch.

2.1 Power-Stage Modeling

To derive a state-space representation for DC-DC converters operating in the continuous conduction mode with fixed-frequency duty-ratio control, we first treat the open-loop sys-

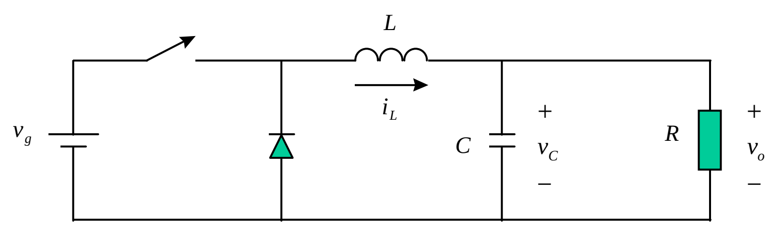

(a)

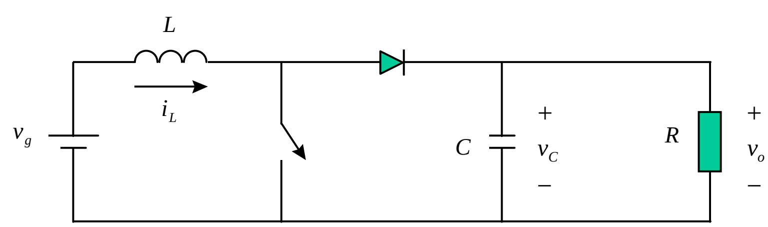

(b)

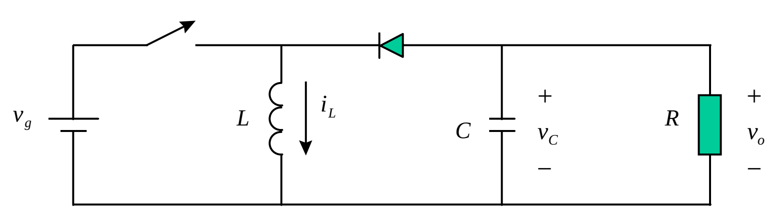

(c)

Figure 2.1: The three basic DC-DC converter configurations: (a) buck converter, (b) boost converter, and (c) buck-boost converter.

tem as a multi-topological or multi-structural system with two circuit configurations. Each configuration describes the system in a sub-interval of time within the switching cycle T. Hence, the period of each switching cycle can be divided into two time intervals: T_1 and T_2. During T_1, the switch is on and the diode is off, and during T_2, the switch is off and the diode is on. In this model we are assuming that the diode and the switch are ideal. The inductor of the power stage has an equivalent series resistance (ESR) R_L and the capacitor has an ESR R_C. The three basic switching converters are shown in Fig. 2.1. The topological sequence of each consists of two linear time-invariant systems described by the following state-space equations:

For the interval T_1

$$\dot{\xi} = A_1^o \xi + B_1^o v_g \tag{2.1}$$

$$v_o = C_1^o \xi \tag{2.2}$$

For the interval T_2

$$\dot{\xi} = A_2^o \xi + B_2^o v_g \tag{2.3}$$

$$v_o = C_2^o \xi \tag{2.4}$$

where ξ is the state vector $[i_L \;\; v_C]^T$ given by

$$v_L(t) = L\frac{di_L(t)}{dt} \quad \text{and} \quad i_C(t) = C\frac{dv_C(t)}{dt} \tag{2.5}$$

Here, A_1^o and A_2^o are 2×2 constant state coefficient matrices composed of the circuit parameters, B_1^o and B_2^o are 2-dim source coefficient column vectors, C_1^o and C_2^o are 2-dim output row vectors, the superscript "o" denotes the open-loop system, v_o is the output voltage across the load resistor R, v_g is the input generator voltage. The A_m^o, B_m^o, and C_m^o for the three types of converters are defined in Appendix A.

It should be pointed out that an additional configuration exists if the system operates in the discontinuous conduction mode. In this case, the current through the inductor reduces to zero and remains zero for a time interval $T_3 = T - T_1 - T_2$, with both the switch and diode being off. The value of the inductance must be sufficiently high to insure that the circuit operates in the continuous mode. It can be shown (Cuk and Middlebrook, 1977) that, for continuous operation, $2L/R$ must be greater than τ_{crit}, where

$$
\begin{aligned}
\tau_{crit} &= (1-D)T \quad \text{for a buck converter,} \\
\tau_{crit} &= D(1-D)T \quad \text{for a boost converter,} \\
\tau_{crit} &= (1-D)^2 T \quad \text{for a buck-boost converter,}
\end{aligned}
$$

and D is the nominal duty ratio. Such a fundamental difference between the two modes of operation necessitates two separate treatments. As mentioned earlier, in this thesis we address the family of basic converters operating only in the continuous conduction mode.

Taking the average of both intervals and summing the results yields the following large-signal continuous-time system

$$\dot{\bar{\xi}} = (A_1^o d + A_2^o d')\,\bar{\xi} + (B_1^o d + B_2^o d')\,\bar{v}_g \tag{2.6}$$

$$\bar{v}_o = (C_1^o + C_2^o)\,\bar{\xi} \tag{2.7}$$

$$d = \frac{T_1}{T_s} \quad \text{and} \quad d' = \frac{T_2}{T_s} = 1 - d \tag{2.8}$$

where $\bar{\xi}$, $\bar{v}_g$, and $\bar{v}_o$ represent the average power-stage states, input voltage, and output voltage, respectively, and d is the duty ratio. Perturbing the above system around the steady-state operating conditions, linearizing, and taking the Laplace transformation of the linearized equations, we obtain the frequency-domain small-signal transfer functions, such as the input-to-output and the duty-ratio-to-output transfer functions. They are used as building blocks to form the regulator transfer functions, such as the loop gain transfer function.

Since the regulator system is periodically driven, it is more accurate to develop a discrete model by representing the system dynamics by an iterative map in which the value of ξ at $t = (n+1)T$ is expressed in terms of the value of ξ at $t = nT$. Such a map will facilitate the investigation of subharmonics and chaos.

The solution of each of the state Equations (2.1)-(2.4) can be expressed in terms of respective transition matrices. Then, the consecutive solutions are "stacked" over a switching period. The result is a discrete-time difference equation, which can be written in state-space form as

$$\xi(n+1) = f(\xi(n), d(n), v_g(n)) = \Phi(d(n))\xi(n) + \Gamma(d(n))v_g(n) \qquad (2.9)$$

$$v_o(n+1) = g(\xi(n), d(n), v_g(n)) = \Psi\xi(n+1) \qquad (2.10)$$

where

$$\Phi(d(n)) = \Phi_2(d'(n)T)\Phi_1(d(n)T), \qquad (2.11)$$

$$\Gamma(d(n)) = \Phi_2(d'(n)T)\int_0^{d(n)T} \Phi_1(\tau)B_1^o d\tau + \int_0^{d'(n)T} \Phi_2(\tau)B_2^o d\tau, \qquad (2.12)$$

$$\text{and} \qquad \Psi = C_2^o. \qquad (2.13)$$

Here, $t(n)$ is the start of the nth switching cycle, $t(n+1)$ is the end of nth switching cycle,

$\xi(n) = \xi(t(n))$, $\xi(n+1) = \xi(t(n+1))$, $T = T_1 + T_2$ is the switching cycle or period, $d(n)$ is the duty ratio at the nth switching cycle, $d'(n) = 1 - d(n)$, and the transition matrices are given by the series

$$\Phi_k(\tau) = e^{A_k^o \tau} = 1 + \sum_{n=1}^{\infty} \frac{(A_k^o)^n \tau^n}{n!} \tag{2.14}$$

where $k = 1,\ 2$. Using the relation

$$\int_0^t e^{A_k^o \tau} B_k^o v_g(n) d\tau = \left[e^{A_k^o t} - I \right] (A_k^o)^{-1} B_k^o v_g(n) \tag{2.15}$$

we rewrite Eq. (2.9) as

$$\begin{aligned} \xi(n+1) &= e^{A_2^o d'(n)T} e^{A_1^o d(n)T} \xi(n) + \left[e^{A_2^o d'(n)T} \left(e^{A_1^o d(n)T} - I \right) (A_1^o)^{-1} B_1^o \right. \\ &+ \left. \left(e^{A_2^o d'(n)T} - I \right) (A_2^o)^{-1} B_2^o \right] v_g(n) \end{aligned} \tag{2.16}$$

Next we consider the closed-loop system of the converter and compensator.

2.2 Compensator Modeling

A DC-DC switch-mode regulator should be designed to remain stable under all operating conditions; have a good regulation, such that the output remains constant if either the input voltage varies or the load changes; and have a good transient response to system disturbances, such as sudden changes in either the input voltage, the load, or both. These requirements are met by designing a feedback system that controls the duty ratio d of the power switch to keep the output constant at all times. As mentioned earlier, when incorporated in a closed-loop feedback system, a DC-DC converter forms a switching-mode regulator. A simple buck

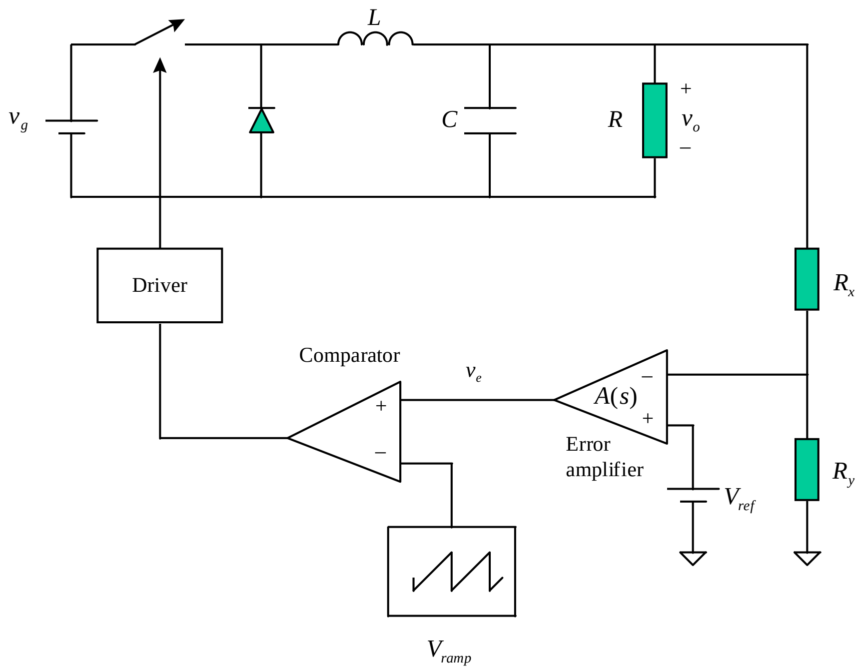

Figure 2.2: Closed-loop buck regulator system.

regulator with feedback control is shown in Fig. 2.2.

The error processor is the feedback compensation network. In designing the feedback loop, one needs to determine the transfer function of each block and optimize the loop transfer function. The small-signal frequency transfer function of the error amplifier $A(s)$ can be found and the loop gain transfer function can be obtained. Using the classical theory of control systems, one can predict the stability of the regulator system.

For the closed-loop system shown in Fig. 2.2, we assume that the mth-order, linear, time-invariant (LTI) error amplifier can be represented in the ith switch configuration in state-space form as

$$\dot{z} = Fz + Gv_o + QV_{ref} \tag{2.17}$$

$$v_e = Hz \tag{2.18}$$

where z is an $m \times 1$ state vector, F is an $m \times m$ constant matrix, G and Q are $m \times 1$ column vectors, H is a $1 \times m$ row vector, V_{ref} is the reference voltage, v_o is the output voltage, and v_e is the output of the error amplifier (control voltage), which is the input to the modulator. We note that, in the frequency domain, m is the number of poles of the compensator transfer function $A(s)$, as shall be seen later. Next, we combine the power circuit and controller to obtain the following state-space model of the closed-loop system:

During the on-time

$$\dot{x} = A_1^c x + B_{g1}^c v_g + B_{r1}^c V_{ref} \tag{2.19}$$

$$v_o = C_1^c x \tag{2.20}$$

$$v_e = H_1^c x \tag{2.21}$$

During the off-time

$$\dot{x} = A_2^c x + B_{g2}^c v_g + B_{r2}^c V_{ref} \tag{2.22}$$

$$v_o = C_2^c x \tag{2.23}$$

$$v_e = H_2^c x \tag{2.24}$$

where

$x = [\xi \quad z]$ and A_m^c, $B_{g_m}^c$, $B_{r_m}^c$, and H_m^c are defined in Appendix B. The superscript "c" denotes the closed-loop system.

Using the same procedure as before, the large-signal continuous-time model can be expressed as

$$\dot{\bar{x}} = (A_1^c d + A_2^c d')\bar{x} + (B_{g1}^c d + B_{g2}^c d')\bar{v}_g + (B_{r1}^c d + B_{r2}^c d')V_{ref} \tag{2.25}$$

$$\bar{v}_o = (C_1^c d + C_2^c d')\bar{x} \tag{2.26}$$

$$\bar{v}_e = (H_1^c d + H_2^c d')\bar{x} \tag{2.27}$$

where $\bar{x}$ and $\bar{v}_e$ represent the average states of the closed-loop system and the average value of the error or control signal, respectively.

The exact discrete model, describing the closed-loop switched-mode converter over a complete cycle, can be readily obtained by stacking the solutions of each switched system over one cycle. The result is

$$\begin{aligned} x(n+1) &= e^{A_2^c d'(n)T} e^{A_1^c d(n)T} x(n) \\ &+ \left[e^{A_2^c d'(n)T}\left(e^{A_1^c d(n)T} - I\right)(A_1^c)^{-1}B_{g1}^c + \left(e^{A_2^c d'(n)T} - I\right)(A_2^c)^{-1}B_{g2}^c\right] v_g(n) \\ &+ \left[e^{A_2^c d'(n)T}\left(e^{A_1^c d(n)T} - I\right)(A_1^c)^{-1}B_{r1}^c + \left(e^{A_2^c d'(n)T} - I\right)(A_2^c)^{-1}B_{r2}^c\right] V_{ref} \end{aligned} \tag{2.28}$$

$$v_o(n+1) = C_2^c x(n+1) \tag{2.29}$$

It follows form Eq. (2.28), that d is an input variable, which can be varied to regulate the system. When d is assigned a fixed value, the system is said to be uncontrolled or open-loop. Note that in this case d is independent of x and the map is linear in x. On the other hand, when d is varied according to x, the system is said to be a closed-loop system, and the resulting map is nonlinear. In practice, the value of d is adjusted via a pulse-width modulator, which turns on the switch at $t = nT$ for a duration $d(n)T$. It should be noted that, because the original system is continuous in nature, this nonlinear map is the Poincaré map of the original system. It gives a sample of the state variables of the system every clock cycle (switching period). A periodic solution of the system appears as a single point or several discrete points in the case of a subharmonic, whereas a chaotic attractor appears as an intricate, multilayered structure. The Poincaré section is a graphical representation as only essential information about the system is retained. Indeed, the samples of the states at the switching cycles, together with the duty ratio, define the original continuous system completely. In other words, the continuous-time behavior can be reconstructed from this information.

2.3 Pulse-Width Modulator Modeling

In most DC-DC switch-mode converters, the output voltage is controlled by comparing it with a reference voltage and using the error to adjust the duty ratio d. Normally, the duty ratio is obtained by comparing the error or control voltage v_e with a fixed-frequency sawtooth voltage V_{ramp}. When the v_e is greater than V_{ramp}, the switch is turned on, and consequently the diode turns off. When v_e is less than V_{ramp}, the switch is turned off, and as a result the diode turns on. In this case, the duty ratio in the nth cycle is the solution of

$$v_e(d(n)T) = V_{ramp}(d(n)T) \tag{2.30}$$

We refer to this equation as the switching condition, which we rewrite as

$$\sigma(x(n), d(n), v_g(n)) = 0 \tag{2.31}$$

On average, the output of the modulator is related to the error signal through

$$d = \frac{1}{V_m}\bar{v}_e \tag{2.32}$$

where $\bar{v}_e$ is the average value of the error or control signal. Note that, in the frequency domain, the describing function of the modulator is simply

$$F_M(s) = 1/V_m \tag{2.33}$$

Clearly, Eqs. (2.28), (2.29), and (2.31) define the complete closed-loop regulator system as a nonlinear discrete time-varying system. We shall use them to predict the bifurcation path of the system, with the input voltage being the bifurcation parameter.

Chapter 3

Stability Analysis

In general, the equilibrium solutions of the map

$$x(n+1) = f(x(n), d(n), u(n)) = \Phi(d(n))x(n) + \Gamma(d(n))u(n) \tag{3.1}$$

$$y(n+1) = g(x(n), d(n), u(n)) = \Psi x(n+1) \tag{3.2}$$

with the general constraint

$$\sigma(x(n), d(n), u(n)) = 0 \tag{3.3}$$

can be obtained by enforcing periodicity. Putting $x_{n+1} = x_n = X$, we obtain

$$X = f(X, D, U) \tag{3.4}$$

$$Y = \Psi X \tag{3.5}$$

where X, D, U, and Y are the equilibrium values. We note that there is only one value of $D \in [0, 1]$ that corresponds to a given equilibrium value (Tse and Adams, 1991). The switching constraint or condition becomes

$$\sigma(X, D, U) = 0 \tag{3.6}$$

To solve for the equilibrium solutions, we substitute for X from Eq. (3.4) into Eq. (3.6) to obtain a nonlinear equation in D. Using a combination of the bisection and Newton-Raphson schemes, we solve for D. Substituting D back into Eq. (3.4), we compute the equilibrium solution X, and from Eq. (3.5) we obtain the output at equilibrium Y.

In the design of any closed-loop system, the most fundamental requirement is stability. In other words, the system should be designed in such a way that any perturbation superimposed on the equilibrium solution will decay with time. In the closed-loop switching converter, feedback compensation is used to shape the frequency response such that it remains stable under all operating conditions. In linear analysis, the relative stability of a feedback system can be inferred from its gain and phase margins. To ensure stable loop response of the switching converter, it is usual to design for a gain margin of at least 6 dB and a phase margin of about 45°.

To determine the stability of the equilibrium solutions, we investigate the linearization of the nonlinear generalized state-space model defined by Eqs. (3.1)-(3.3). To this end, we consider deviations from the nominal values and let

$$x = X + \hat{x}, \quad d = D + \hat{d}, \quad u = \hat{u} + U, \quad \text{and} \quad y = Y + \hat{y} \tag{3.7}$$

Substituting Eq. (3.7) into Eqs. (3.1)-(3.3), expanding the result in multi-variable Taylor series, and keeping the linear terms in the deviations, we obtain

$$\hat{x}_{n+1} \approx \frac{\partial f}{\partial x}\hat{x}_n + \frac{\partial f}{\partial d}\hat{d}_n + \frac{\partial f}{\partial u}\hat{u}_n \tag{3.8}$$

$$\hat{y}_n \approx \frac{\partial g}{\partial x}\hat{x}_n + \frac{\partial g}{\partial d}\hat{d}_n + \frac{\partial g}{\partial u}\hat{u}_n \tag{3.9}$$

$$0 \approx \frac{\partial \sigma}{\partial x}\hat{x}_n + \frac{\partial \sigma}{\partial d}\hat{d}_n + \frac{\partial \sigma}{\partial u}\hat{u}_n \tag{3.10}$$

The partial derivatives in Eqs. (3.8)-(3.10) are functions of X, D, and U. This linearized model is itself in generalized state-space form, with the deviations $\hat{x}$, $\hat{d}$, $\hat{u}$, and $\hat{y}$ constituting the state variables, auxiliary variable, input, and output, respectively. The major simplification though is that this description is linear and time-invariant because all of the coefficients are known functions of the nominal solution. The linearity allows us to solve explicitly the constraint expression in Eq. (3.10) for the auxiliary variable $\hat{d}$. The result is

$$\hat{d} = -\left[\frac{\partial \sigma}{\partial d}\right]^{-1}\left[\frac{\partial \sigma}{\partial x}\hat{x}_n + \frac{\partial \sigma}{\partial u}\hat{u}_n\right] \tag{3.11}$$

Using Eq. (3.11) to eliminate the auxiliary variable in Eqs. (3.8) and (3.9), we obtain the following linear description in ordinary state-space form

$$\hat{x}_{n+1} \approx \hat{A}\hat{x}_n + \hat{B}\hat{u}_n \tag{3.12}$$

$$\hat{y}_n \approx \hat{C}\hat{x}_n + \hat{D}\hat{u}_n \tag{3.13}$$

where

$$\hat{A} = \frac{\partial f}{\partial x} - \frac{\partial f}{\partial d}\left[\frac{\partial \sigma}{\partial d}\right]^{-1}\frac{\partial \sigma}{\partial x}, \qquad \hat{B} = \frac{\partial f}{\partial u} - \frac{\partial f}{\partial d}\left[\frac{\partial \sigma}{\partial d}\right]^{-1}\frac{\partial \sigma}{\partial u} \tag{3.14}$$

$$\hat{C} = \frac{\partial g}{\partial x} - \frac{\partial g}{\partial d}\left[\frac{\partial \sigma}{\partial d}\right]^{-1}\frac{\partial \sigma}{\partial x}, \qquad \hat{D} = \frac{\partial g}{\partial u} - \frac{\partial g}{\partial d}\left[\frac{\partial \sigma}{\partial d}\right]^{-1}\frac{\partial \sigma}{\partial u} \tag{3.15}$$

The eigenvalues, characteristic or Floquet multipliers, of $\hat{A}$ determine the stability of the linearized system. The natural response of the system will decay asymptotically to zero if and only if all of the Floquet multipliers have magnitudes less than unity; that is, if and only if they lie strictly inside the unit circle in the complex plane. This condition is therefore necessary and sufficient for asymptotic stability. For the forced response, exponential stability of the natural response turns out to be sufficient to guarantee a bounded response to bounded inputs (Kassakian, Schlecht, and Verghese, 1991).

A number of examples are given to demonstrate the application of the generalized procedure presented in the previous sections. The first example is a single-loop buck converter operating in continuous conduction mode with proportional feedback voltage control and constant-frequency duty-ratio control. The analysis of this example is carried out in detail to show how the generalized method can be applied. The results indicate that this simple circuit possesses complex behavior, including subharmonics and chaos. After that, the same converter is studied with integral (I), proportional-integral (PI), and proportional-integral-derivative (PID) feedback control.

3.1 Proportional Control

The DC-DC buck (step down) converter shown in Fig. 2.2 employs a voltage feedback control loop. The power stage has the following component parameters: $L = 50$mH, $C = 100\mu$F, $R_L = 30$mΩ, $R_C = 50$mΩ, $v_g = 20V \sim 40$V, and $R = 5\Omega$. The switching frequency

$f_s = 1/T = 100$kHz. It is readily verified that the value of $2L/R$ is large enough over the whole range of input voltage v_g to ensure a continuous mode of operation. For this system $\omega_s = 2\pi f_s$, $\omega_0 = 1/\sqrt{LC}$, and $\omega_{ESR} = 1/(R_C C)$. A fraction of the output voltage, namely k, is compared with a reference voltage V_{ref}, where $k = R_y/(R_x + R_y) = 1/3$. The resulting error voltage is amplified in the error amplifier by a gain h. The resulting control or error signal v_e is then compared with a ramp signal V_{ramp} to generate the duty-ratio function.

The switched state-space representation of the closed-loop system is exactly as in Eqs. (2.1)-(2.4). The nonlinear map for this specific system is also the same as the map defined in Eq. (2.16). The switching condition is defined through feedback proportional control as

$$\sigma(x(n), d(n), v_g(n)) = v_e(d(n)T) - v_{ramp}(d(n)T) = 0 \tag{3.16}$$

or

$$h(V_{ref} - kv_o(d(n)T)) - V_m d(n) = 0 \tag{3.17}$$

where

$$v_o(d(n)T) = C_1^o x(d(n)T) = C_1^o \left[e^{A_1^o d(n)T} x(n) + \left(e^{A_1^o d(n)T} - I \right) (A_1^o)^{-1} B_1^o v_g \right] \tag{3.18}$$

Using the average model (2.25)-(2.27), we plot in Fig. 3.1 the loop gain of the closed-loop regulator system for three different values of the controller gain h. It follows from the corresponding phase and gain margins for each case that the closed-loop system is stable for the whole operating range of h. However, this condition is at variance with predictions of the present model, as discussed next.

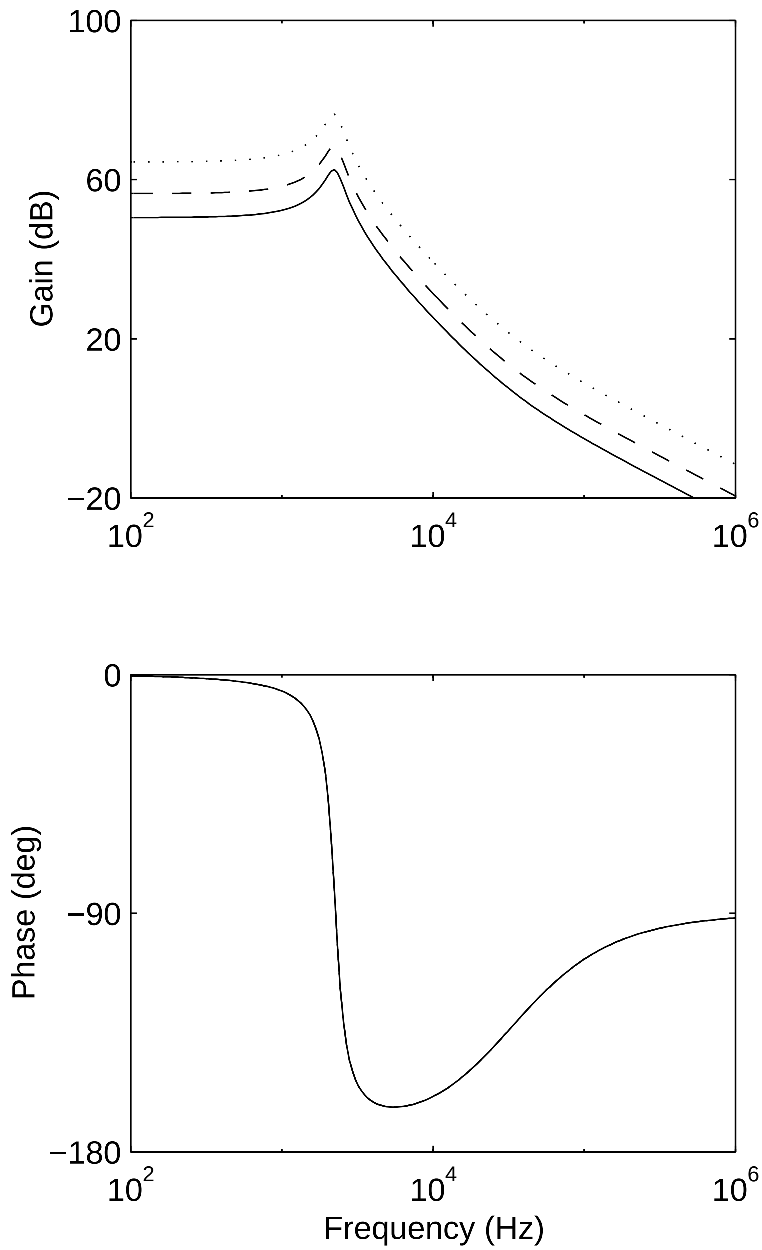

Figure 3.1: Loop gain for different values of h for $v_g = 30$V. (——) $h = 100$, $(---)$ $h = 200$, and $(\cdots\cdots)$ $h = 500$.

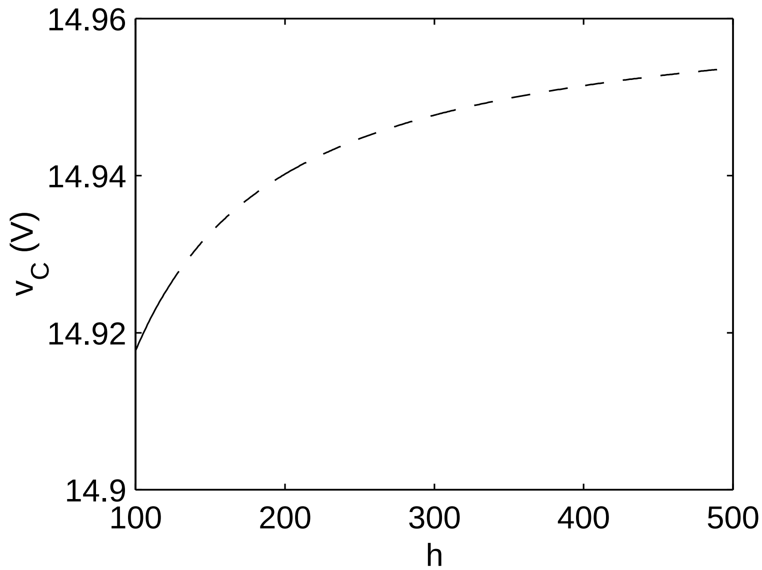

Figure 3.2: Variation of v_C at equilibrium with h for $v_g = 30$V. (——) stable solution and (– – –) unstable solution.

In Fig. 3.2 we show the voltage across the output filter capacitor v_C at equilibrium. The solid line denotes stable period-one solutions, and the dashed line denotes unstable period-one solutions. When $h < 120$, the eigenvalues are inside the unit circle and hence the period-one solution is stable. As h is increased beyond 120, one of the Floquet multipliers exits the unit circle through -1, indicating a period doubling bifurcation. Consequently, the period-one solution loses stability and the period of the response is doubled.

Next, we present in Fig. 3.3 the bifurcation diagram obtained before and after the period-doubling bifurcation. Starting with an initial state x_0 and a given h, we first solve Eq. (3.17) numerically using the bisection method to obtain an initial guess for d_0 and improve on this guess using a Newton-Raphson scheme. Then, we substitute the obtained value of d_0 into the map (2.28) to determine x_1. Using x_1, we determine d_1 and then substitute the results back into the map to obtain x_2. The iterations are continued for a thousand times. The first 500 iterates are discarded and the last 500 iterates are plotted for the given h. Next, h is incremented by a small amount and the procedure is repeated. For values of h below 120, the bifurcation diagram consists of a single point for each value of h, which indicates a period-one solution. As h is increased past 120, the stable period-one solution undergoes a period-doubling bifurcation with a Floquet multiplier exiting the unit circle through -1, as aforementioned, resulting in the creation of two stable period-two orbits and an unstable period-one orbit. Further increase in h leads to a cascade of period-doubling bifurcations, culminating in a chaotic attractor. It is clear from Fig. 3.3 that there exist many small intervals of h within the chaotic region for which the response is periodic, repeating exactly after m iterations. In other words, there are many small windows of periodic solutions.

We have simulated the steady-state waveforms for various values of h belonging to period-1, 2, 4, 8, and chaotic solutions. Figure 3.4(a-e) shows the steady-state waveforms of the closed-loop system with $h = 100$, 200, 300, 350, and 400, respectively. The two-dimensional projections of the phase portraits on the i_L-v_C plane corresponding to these five cases are also shown. They demonstrate clearly the period-1, period-2, period-4, period-8, and chaotic orbits. The power spectrum density for each of these cases is also shown.

To confirm the chaotic nature of the orbit at $h = 400$, we chose two initial conditions close to the attractor; the separation d_0 between them is 10^{-6}. We plot in Fig. 3.5 the separation d_k with the iterate number k. Clearly, d_k increases exponentially for $k < 35$ before leveling

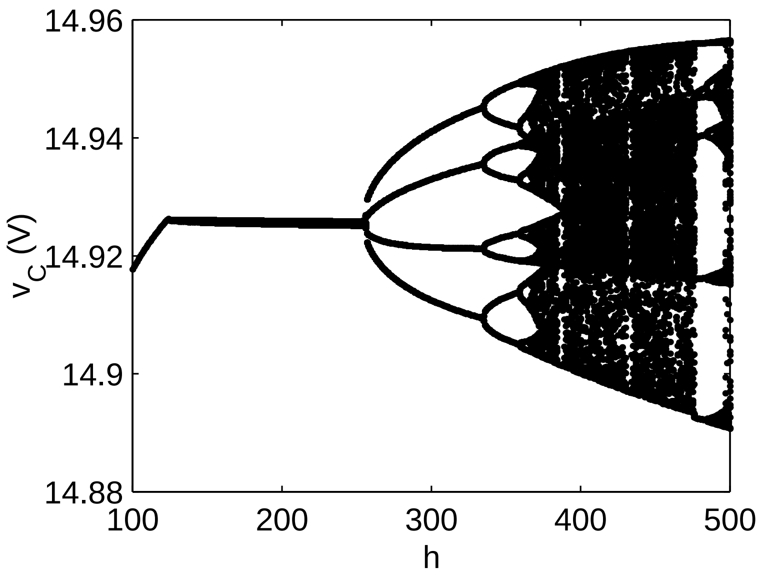

Figure 3.3: Bifurcation diagram with h as the control parameter when $v_g = 30$V.

off. This leveling off occurs because d_k cannot grow beyond the size of the attractor. On the average, the growth of d_k in the intermediate regime can be modeled as

$$d_k = d_0 e^{\gamma k} \tag{3.19}$$

where γ is the Lyaponov exponent. From the figure, we find that $\gamma \approx 0.16$, which confirms the chaotic nature of the attractor. In Fig. 3.6 we show the return map by plotting $v_C(n+1)$ versus $v_C(n)$. We show 2,000 iterates on the attractor.

To compare different regulator systems with different compensation networks, the control (design) parameter should be independent from the compensator design. A good choice would be either the input voltage v_g or the load resistance R. Hence we repeated the calculations for the same proportional feedback system with the input voltage as the control

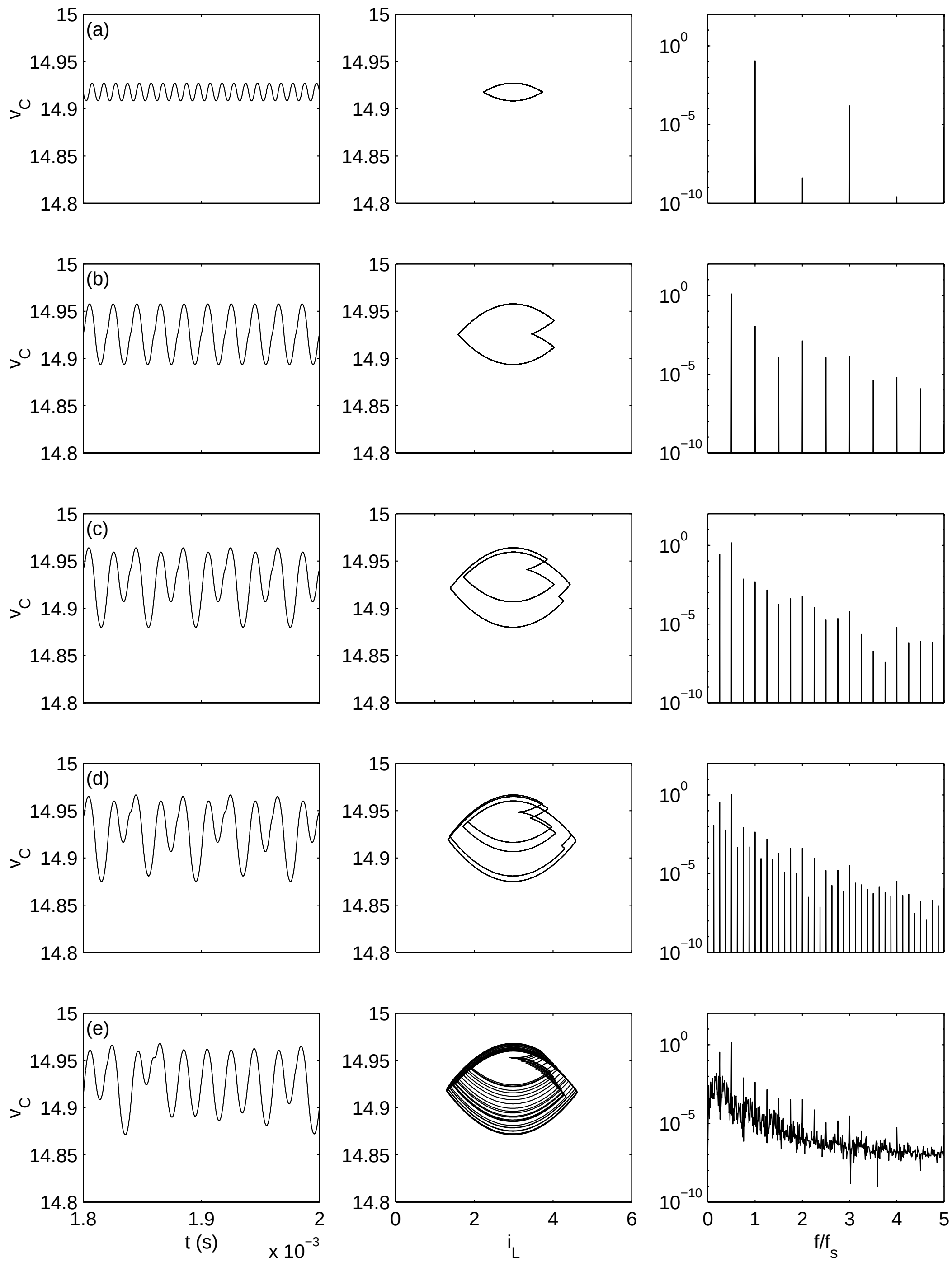

Figure 3.4: Long-time history, state-plane and power spectral density of the voltage across the capacitor for different values of h: (a) 100, (b) 200, (c) 300, (d) 350, and (e) 400 when $v_g = 30\text{V}$.

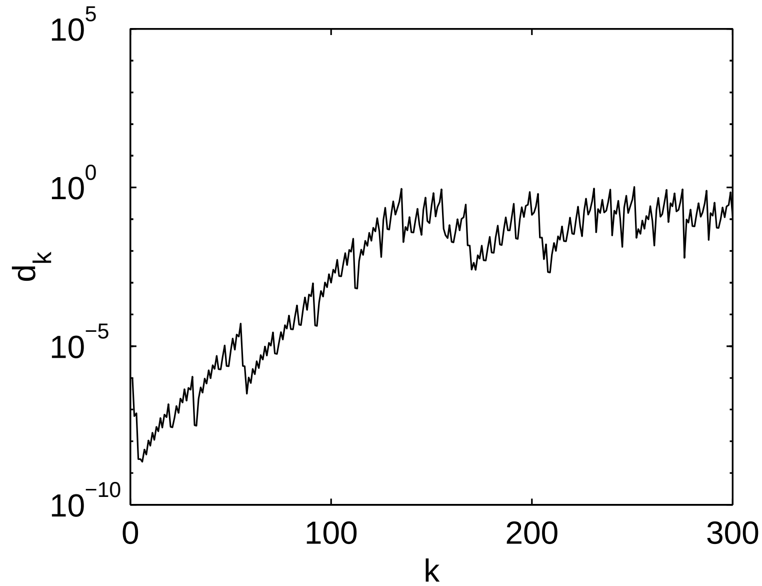

Figure 3.5: Sensitivity to initial conditions on the chaotic attractor realized for $h = 400$.

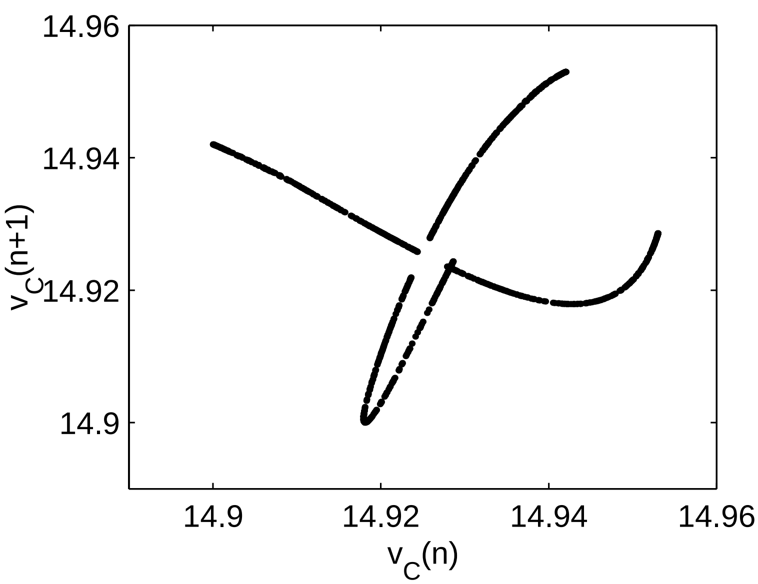

Figure 3.6: Attractor of the nonlinear map for $h = 400$.

parameter.

Using state-space averaging techniques, we plot in Fig. 3.7 the loop gain of the closed-loop system for different values of the input voltage. Again, it is clear from the phase and gain margins that the closed-loop system is stable on the slow scale (averaged behavior) for the whole range of the operating parameter.

The period-one equilibrium solutions and their stability are shown in Fig. 3.8 for $h = 200$, and the resulting bifurcation diagram is shown in Fig. 3.9. We note that in this bifurcation diagram the period-doubling route to chaos is from right to left, as opposed to the one obtained earlier when h was the control parameter. This is interesting since increasing both h and v_g have the same effect on the average loop gain of the closed-loop system. However, their effect on the fast scale is exactly the opposite.

Figure 3.10(a-e) shows the steady-state waveforms of the closed-loop system with $v_g = 50$, 40, 27, 26, and 24V, respectively. The two-dimensional projections of the phase portraits on the i_L-v_C plane corresponding to these five cases are also shown. They demonstrate clearly the period-1, period-2, period-4, period-8, and chaotic orbits. The power spectrum density for each of these cases is also shown.

For a fixed input voltage, it can be easily explained why the route to chaos is from lower gains to higher gains when the controller gain is used as the control parameter. The higher the gain is, the less the high-frequency components get attenuated. Hence, their effect is larger. The power spectrum of the response in the chaotic region is wide band, unlike that of

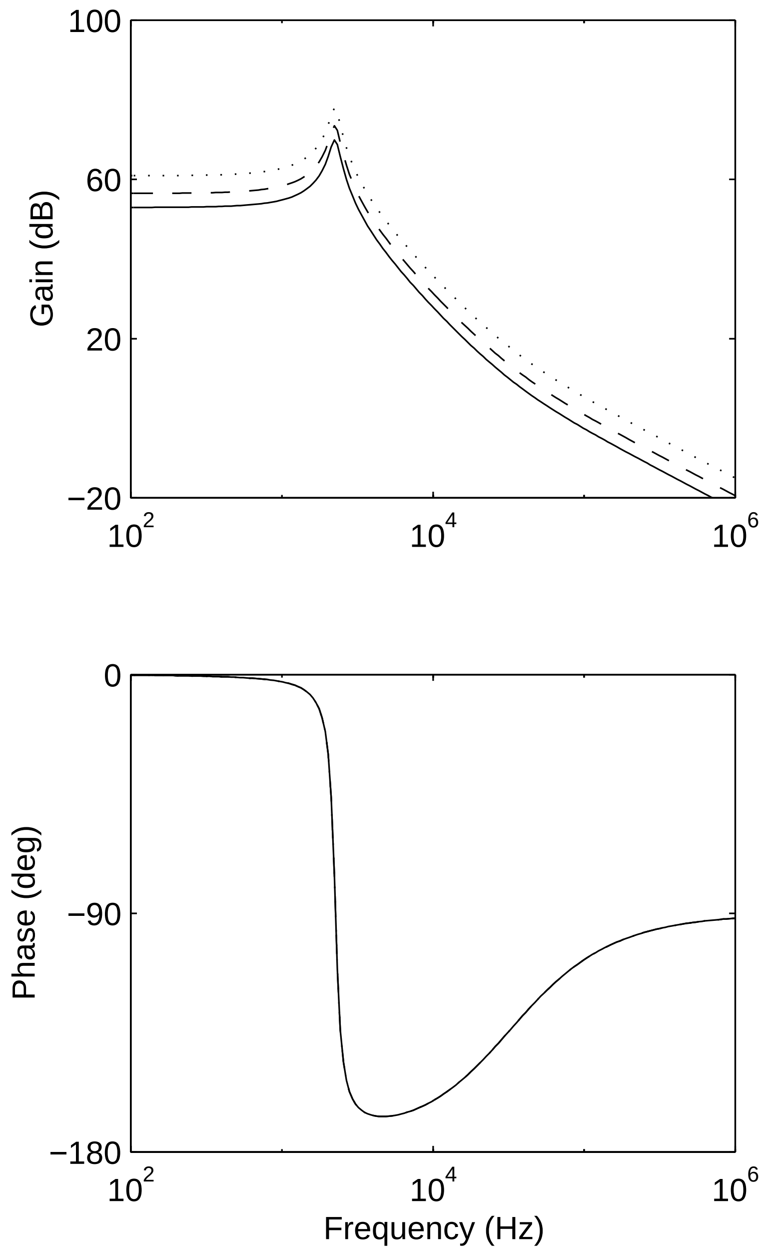

Figure 3.7: Loop gain for different values of v_g for $h = 200$. (——) $v_g = 20$V, (– – –) $v_g = 30$V, and $(\cdot\cdot\cdot\cdot\cdot)$ $v_g = 50$V.

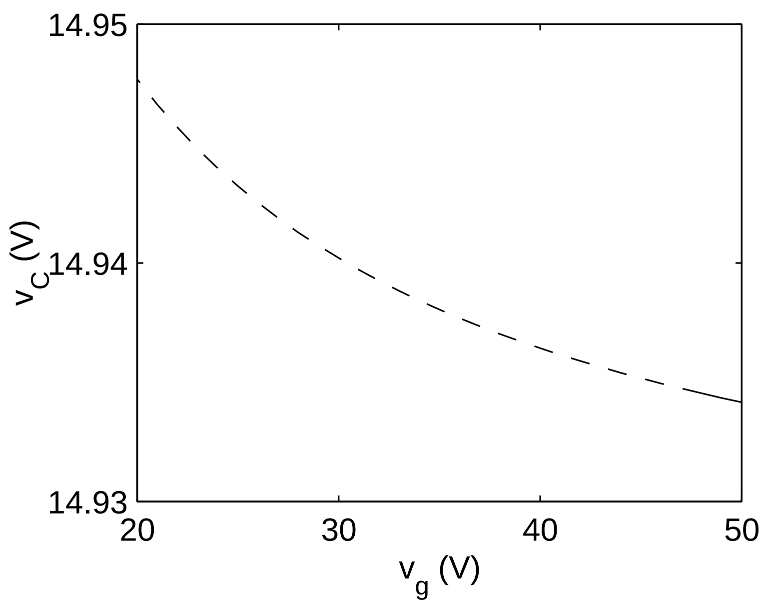

Figure 3.8: Period-one equilibrium solutions for different values of v_g for $h = 200$. (——) stable solution and (– – –) unstable solution.

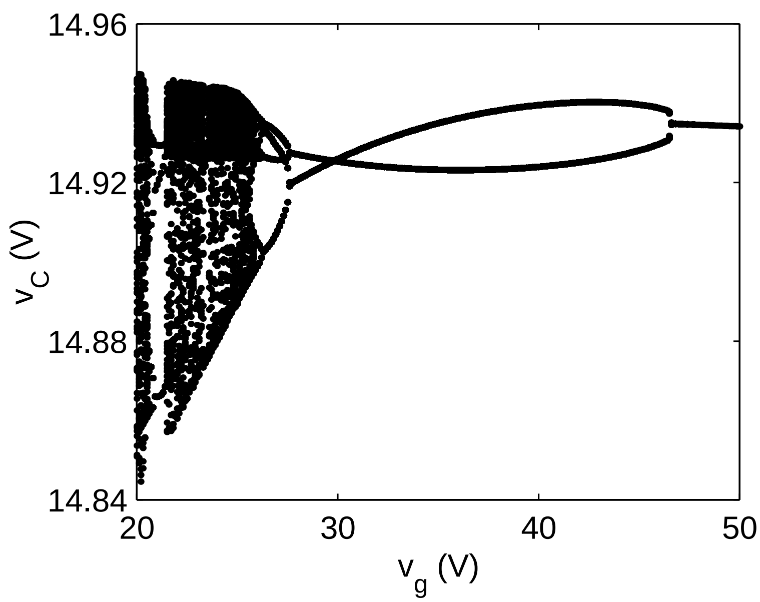

Figure 3.9: Bifurcation diagram of the regulator system with proportional control with v_g as the control parameter.

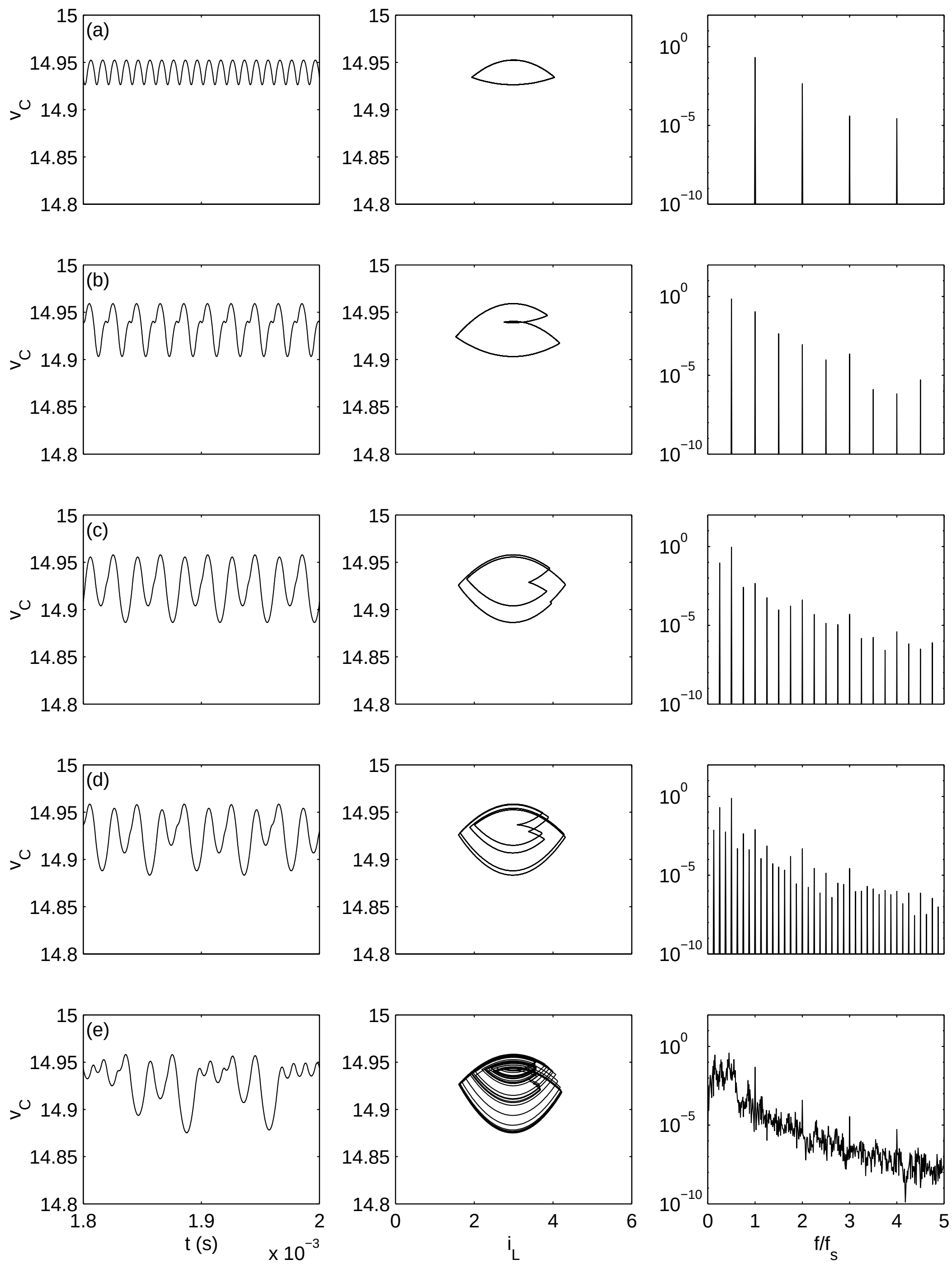

Figure 3.10: Long-time history, phase-plane and power spectral density of the voltage across the capacitor for different values of v_g: (a) 50V, (b) 40V, (c) 27V, (d) 26V, and (e) 24V.

the period-one solution, which is characterized by a fundamental at the switching frequency and its higher harmonics. Thus, the higher the controller gain and hence the higher the loop gain, the more likely the instability will occur on the fast scale. However, it is not clear why the period-doubling route to chaos in the case of a fixed controller gain and v_g being the control parameter is in the opposite direction of that with the gain being the control parameter.

In conclusion, the input voltage and the gain of the proportional controller, which determine the crossover frequency of the loop gain, which in turn determine the bandwidth of the regulator system, act on the stability in opposite directions. While increasing the loop gain by increasing the gain of the feedback controller has a destabilizing effect on the period-one operation, increasing the loop gain by increasing the input voltage at the source end has a stabilizing effect.

It is worth pointing out that, for a gain $h = 100$ and low input voltages, the crossover frequency of the loop gain is below half the switching frequency as recommended by the designers of switching converters, yet the system is unstable on the fast scale. Moreover, when the crossover is greater than half the switching frequency for high input voltages, the operation is stable and period-one. This contradicts the common design practice in which the system bandwidth is limited to half the switching frequency.

In summary, the present results indicate that subharmonics and more interestingly chaos are present in a simple buck converter operating in closed-loop. Examining the loop gain reveals that high-frequency components near the switching frequency are not sufficiently attenuated by the proportional control. Thus, it would be natural to use a low-pass controller to highly attenuate the high-frequency components. One simple choice would be to use an integrator, as discussed next.

3.2 Integral Control

The transfer function for this type of compensator is given by

$$A(s) = \frac{h}{s} \tag{3.20}$$

which can be expressed in the time domain as

$$\dot{z} = 0 \cdot z - kv_o + V_{ref} \tag{3.21}$$

$$v_e = hz \tag{3.22}$$

The switching condition in this case is

$$h\,[0 \quad 0 \quad 1]\left[e^{A_1^c d(n)T} x(n) + \left(e^{A_1^c d(n)T} - I\right)(A_1^c)^{-1}(B_{g1}^c v_g + B_{r1}^c V_{ref})\right] - V_m d(n) = 0 \tag{3.23}$$

The loop gains of the closed-loop system for $h = 200$ and different values of the input voltage are shown in Fig. 3.11. It follows from the loop gain that frequency components higher than half the switching frequency are attenuated by at least 60 dB. As a result, one would predict that chaos with its route would disappear. Indeed, as seen in Fig. 3.12, the equilibrium solutions are stable for the whole range of the operating parameter.

To confirm that the high-frequency components are responsible for the cause of the chaotic

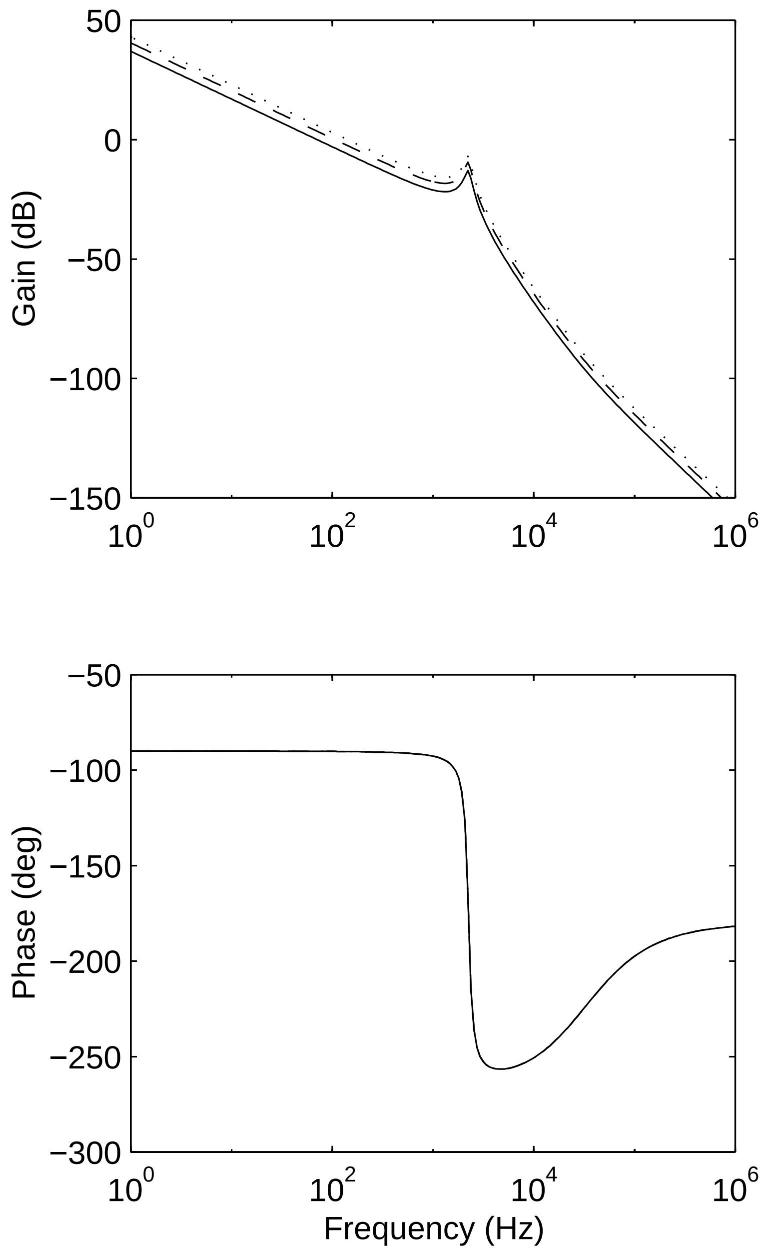

Figure 3.11: Loop gain of the averaged regulator system with integral control for different values of input voltage. (——) $v_g = 20$V, $(- - -)$ $v_g = 30$V, and $(\cdots\cdots)$ $v_g = 40$V.

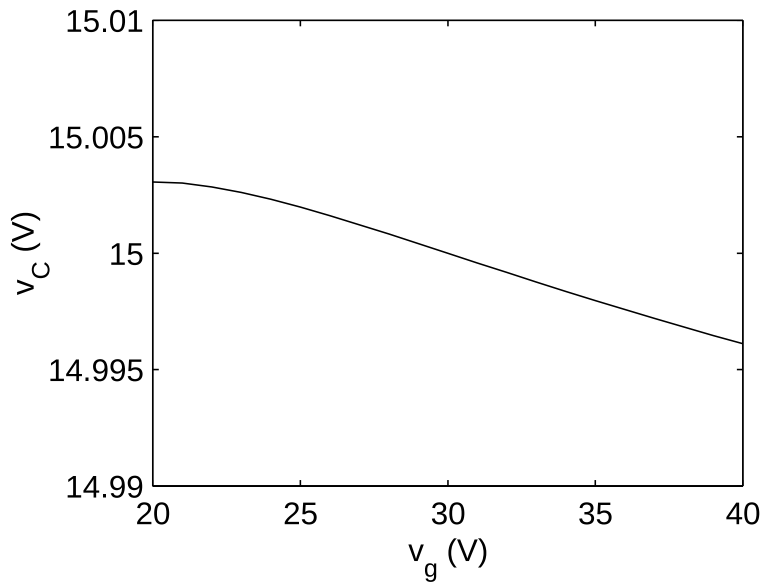

Figure 3.12: Period-one equilibrium solutions of the regulator system with integral control. (——) stable solution and (– – –) unstable solution.

behavior, we consider next a PI controller where, in contrast to the integral controller, high frequencies are not well attenuated.

3.3 Proportional-Integral Control

The transfer function for this controller is given by

$$A(s) = \frac{\omega_I (s/\omega_z + 1)}{s} \tag{3.24}$$

where $\omega_I = 100\,\omega_{ESR}$ and $\omega_z = 0.1\,\omega_0$. We express this controller in the time domain as

$$\dot{z} = 0 \cdot z - kv_o + V_{ref} \tag{3.25}$$

$$v_e = \omega_m \left(\omega_z z + kv_o + V_{ref}\right) \tag{3.26}$$

The switching condition in this case is

$$\begin{aligned} &\omega_m \left[-kC_1^o \quad \omega_z\right] \left[e^{A_1^c d(n)T} x_n + \left(e^{A_1^c d(n)T} - I\right) (A_1^c)^{-1} (B_{g1}^c v_g + B_{r1}^c V_{ref})\right] \\ &+\omega_m V_{ref} - V_m d(n) = 0 \end{aligned} \tag{3.27}$$

where $\omega_m = \omega_I/\omega_z$.

The loop gains for different values of input voltage v_g are shown in Fig. 3.13. The averaged behavior is stable for the whole input voltage range, as clearly seen form the phase and gain margins of the loop gain. However, Figs. 3.14 and 3.15 show that the period-one solution loses stability on the fast scale via a period-doubling route to chaos.

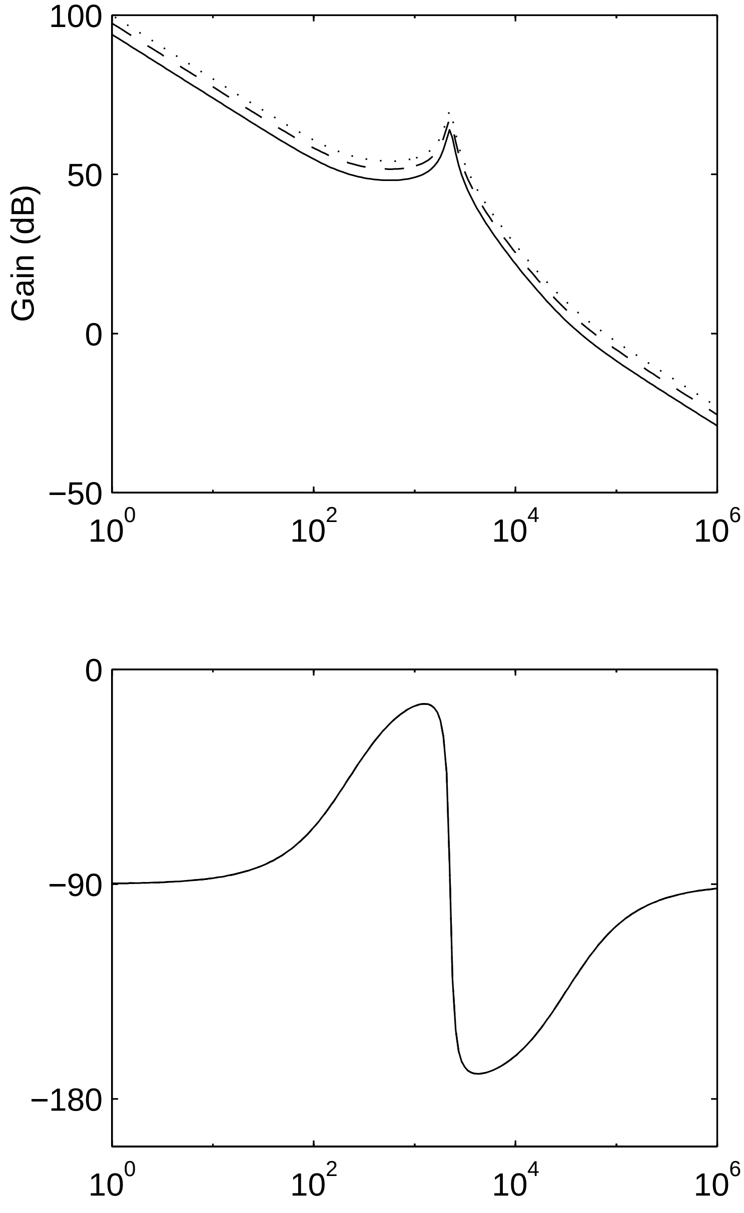

Figure 3.13: Loop gain with proportional-integral control for different values of the input voltage. (——) $v_g = 20$V, ($---$) $v_g = 30$V, and ($\cdots\cdots$) $v_g = 40$V.

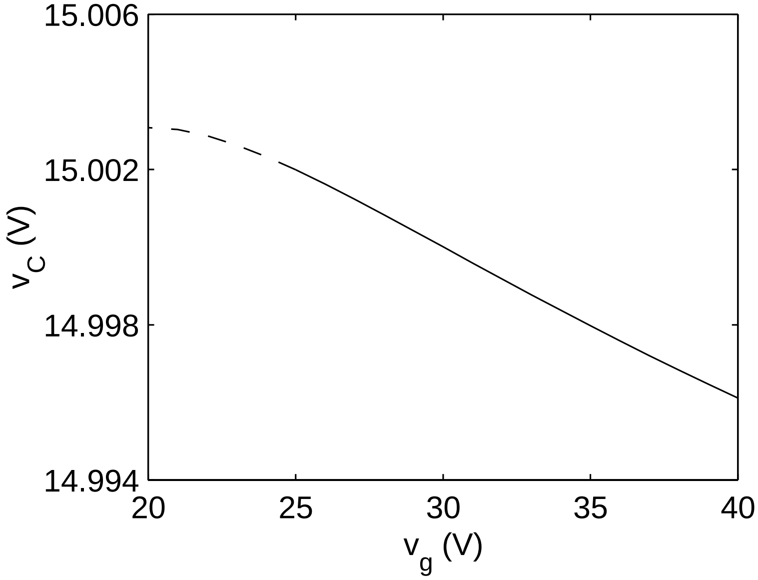

Figure 3.14: Period-one equilibrium solutions of the regulator system with proportional-integral control. (——) stable solution and (– – –) unstable solution.

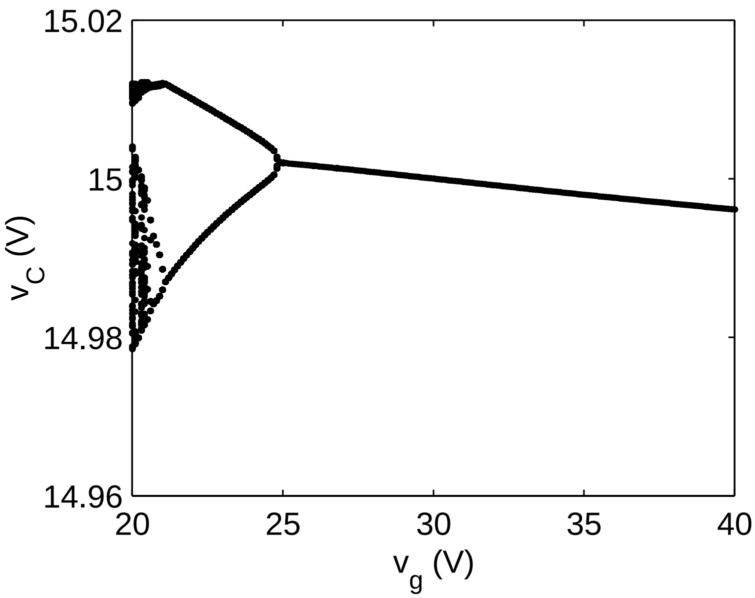

Figure 3.15: Bifurcation diagram with v_g as the control parameter.

We note that Integral and Proportional-Integral controllers are not used in practice. They have a very major drawback. The transient response of the closed-loop system is very poor due to the narrow bandwidth of the loop gain. That is why in practice a PID-type controller is used in order to cross the 0 dB gain at higher frequencies, thereby yielding higher a bandwidths and consequently a faster transient response.

3.4 PID Control

The transfer function of this controller is

$$A(s) = \omega_m \frac{(s/\omega_{z1}+1)(s/\omega_{z2}+1)}{s(s/\omega_{p1}+1)(s/\omega_{p2}+1)} \tag{3.28}$$

where $\omega_I = 96\,\mathrm{dB}$, $\omega_m = \frac{\omega_I \omega_{p1}\omega_{p2}}{\omega_{z1}\omega_{z2}}$, $\omega_{z1} = 0.5\,\omega_{ESR}$, $\omega_{z2} = 1.1\,\omega_0$, $\omega_{p1} = \omega_{ESR}$, and $\omega_{p2} = 0.5\,\omega_s$. The state-space representation of this controller is

$$\dot{z} = \begin{bmatrix} 0 & 1 & 0 \\ 0 & 0 & 1 \\ 0 & -\omega_{p1}\omega_{p2} & -(\omega_{p1}+\omega_{p2}) \end{bmatrix} z + \begin{bmatrix} 0 \\ 0 \\ -k \end{bmatrix} v_o + \begin{bmatrix} 0 \\ 0 \\ 1 \end{bmatrix} V_{ref} \tag{3.29}$$

$$v_e = \begin{bmatrix} \omega_{z1}\omega_{z2} & (\omega_{z1}+\omega_{z2}) & 1 \end{bmatrix} z \tag{3.30}$$

The loop gain transfer function is shown in Fig. 3.16. It is clear that the slow dynamics of the system are stable for the entire range of the input voltage variation. The switching condition in this case is

$$\omega_m \begin{bmatrix} 0 & 0 & \omega_{z1}\omega_{z2} & (\omega_{z1}+\omega_{z2}) & 1 \end{bmatrix}$$

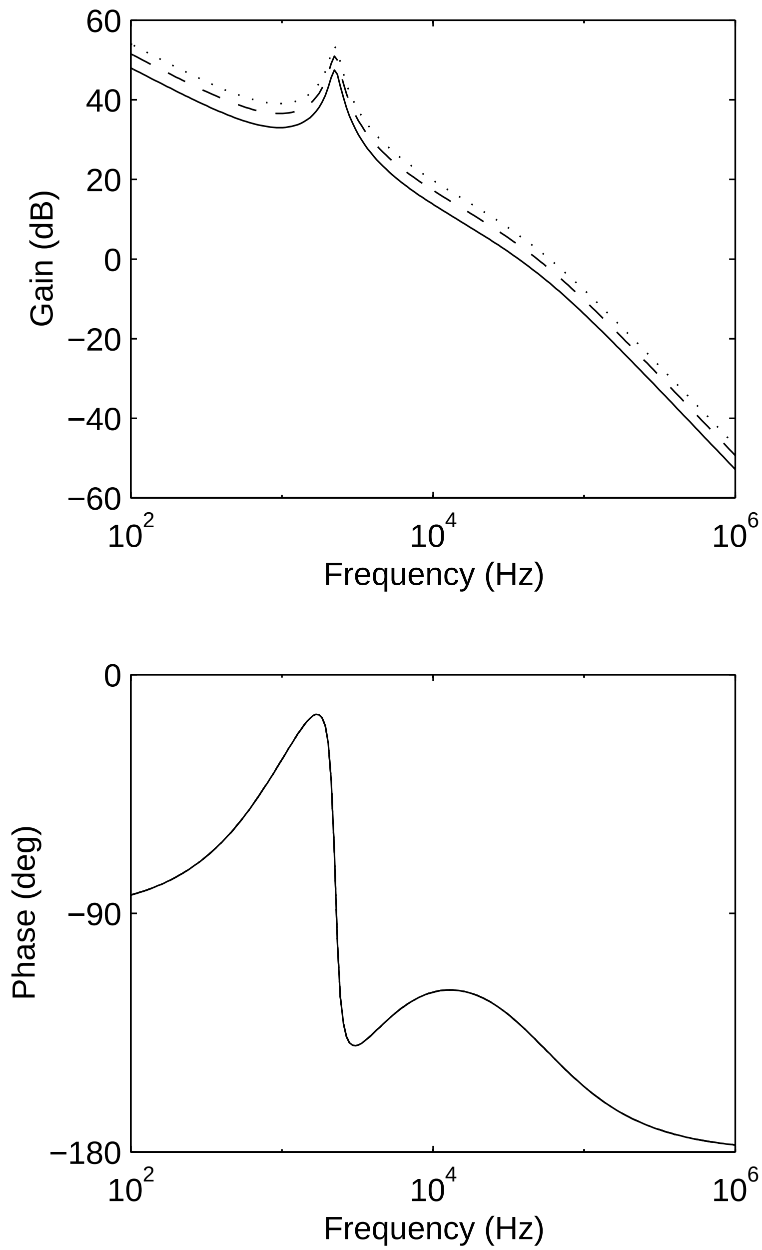

Figure 3.16: Loop gain transfer function with PID control for different values of the input voltage. (——) $v_g = 20$V, (− − −) $v_g = 30$V, and ($\cdot\cdot\cdot\cdot\cdot$) $v_g = 40$V.

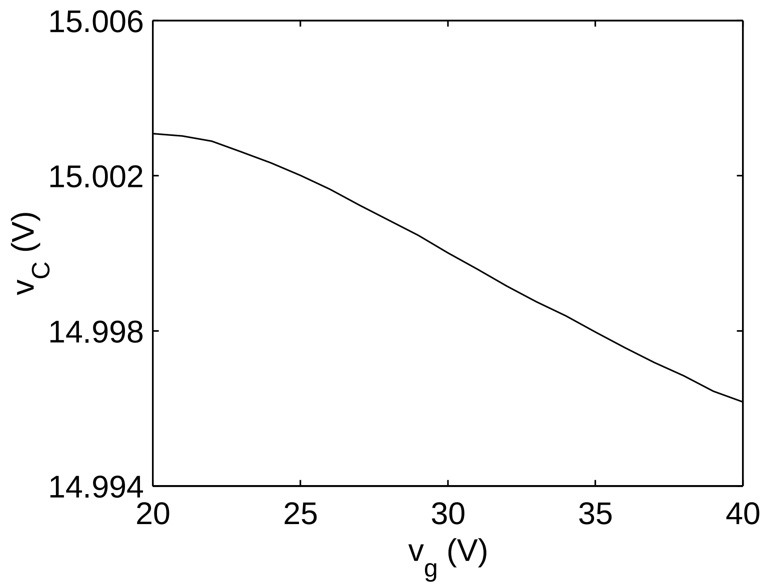

Figure 3.17: Period-one equilibrium solutions of the closed-loop system with PID control for $\omega_I = 96\,\mathrm{dB}$. (——) stable solution and (– – –) unstable solution.

$$\left[e^{A_1^c d(n)T} x(n) + \left(e^{A_1^c d(n)T} - I\right)(A_1^c)^{-1}(B_{g1}^c v_g + B_{r1}^c V_{ref})\right] - V_m d(n) = 0 \quad (3.31)$$

The period-one solution for the system is shown in Fig. 3.17. It is clear that the operation is stable for the controller gain chosen. However, increasing the controller gain by only 4 dB, we find that the instability appears for low input voltages, as shown in Figs. 3.18 and 3.19.

Hence, as shown from the results for the PID controller case, high frequency instability does exist in voltage-mode regulators. The existing averaged-time techniques widely used in the analysis and design of voltage-mode regulators neglect this high frequency effect and as a result give an incomplete stability predictions of the regulator system.

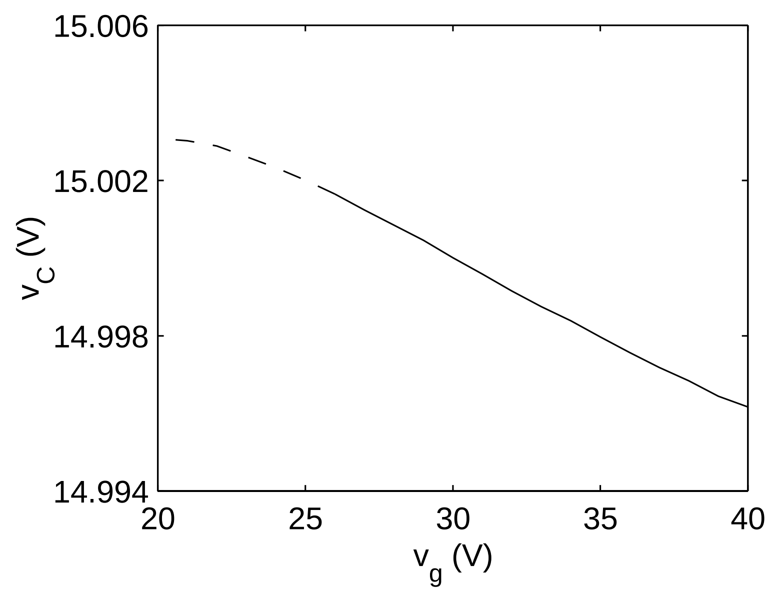

Figure 3.18: Period-one equilibrium solutions of the PID-controlled regulator system with $\omega_I = 100\,\mathrm{dB}$. (——) stable solution and (– – –) unstable solution.

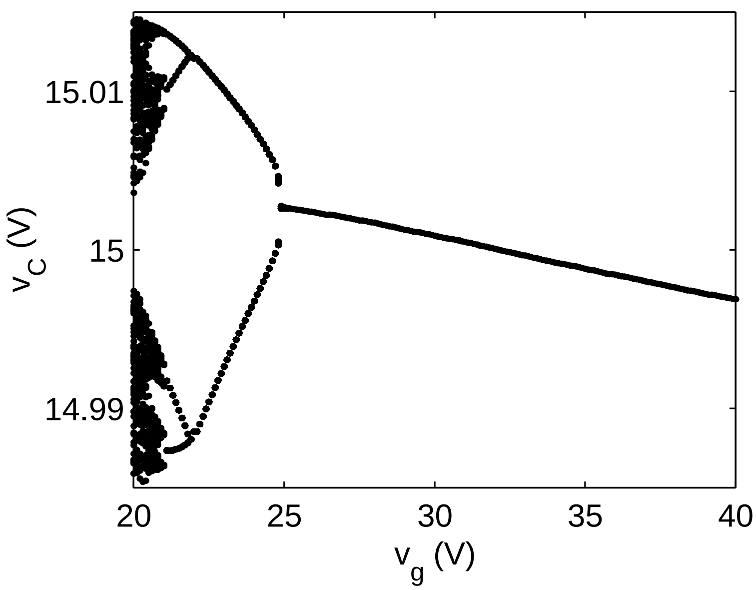

Figure 3.19: Bifurcation digram with v_g as the control parameter with PID control for $\omega_I = 100\,\mathrm{dB}$.

Chapter 4

Filter-Regulator Interactions

An input filter is often required between a switching regulator and its power source. If the input source to the regulator were ideal, then there would be no concern; an ideal source would have no impedance and would remain unperturbed regardless of the input current waveform of the switching regulator. However, in reality, input sources are non-ideal. In order to prevent the input current waveform of the switching regulator from interfering with the source and to preserve the integrity of the source for other equipment that may be operating from a common input power bus, the switching regulator must include appropriate input electromagnetic interference (EMI) filtering. The input filter is also required to isolate the source voltage transients so as not to degrade the performance of the switching regulator. In the next section we present the filter-regulator model by modeling the filter first, then augmenting the filter model with the regulator model derived in Chapter 2 to yield the complete model of the interconnected system of the filter and the regulator.

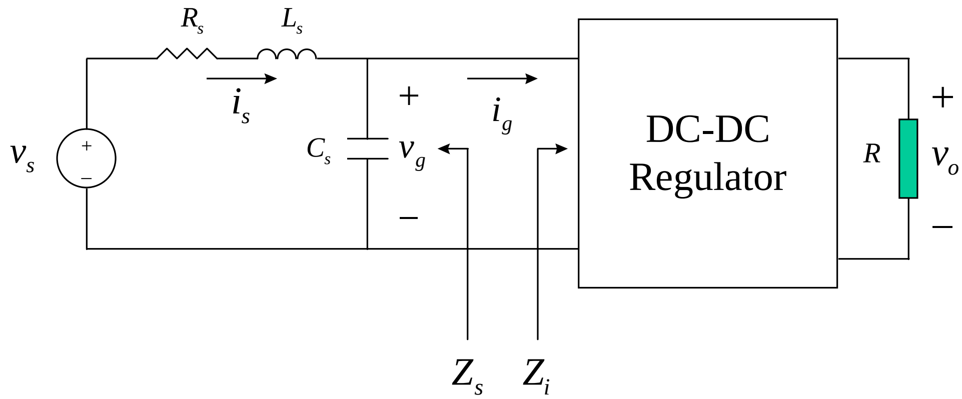

Figure 4.1: Filter-regulator system circuit model.

4.1 Input-Filter Modeling

In Fig. 4.1, we show a circuit model for a DC-DC regulator with a second-order input EMI filter. The filter consists of an inductance L_s and a capacitance C_s. For simplicity, the total effective impedance of the source v_s is modeled as a single effective source resistance R_s, which consists of the source resistance and the series resistance of the inductor. In general, the values of L_s and C_s are large enough to dominate the reactive impedance of the source. This will adequately attenuate the interference due to the signals at the switching frequency and its higher harmonics. Writing down the differential equations governing the dynamics of the filter inductor current and capacitor voltage, we obtain

$$\frac{di_s}{dt} = \frac{1}{L_s}\left(-R_s i_s - v_g + v_s\right) \tag{4.1}$$

$$\frac{dv_g}{dt} = \frac{1}{C_s}\left(i_s - i_g\right) \tag{4.2}$$

where i_s is the current through the filter inductor, v_g is the voltage across the filter capacitor and at the same time the input voltage to the regulator, and i_g is the input current to the regulator. The latter is equal to the power stage inductor current for all types of converters during the on-time, and for the boost converter during the off-time. For the buck and buck-boost converters, it is zero during the off-time.

Having the filter states defined, one completely defines the state-space representation of the interconnected system of the input filter and the regulator as

During the on-time

$$\dot{\zeta} = A_1^i \zeta + B_{s1}^i v_s + B_{r1}^i V_{ref} \tag{4.3}$$

$$v_o = C_1^i \zeta \tag{4.4}$$

$$v_e = H_1^i \zeta \tag{4.5}$$

During the off-time

$$\dot{\zeta} = A_2^i \zeta + B_{s2}^i v_s + B_{r2}^i V_{ref} \tag{4.6}$$

$$v_o = C_2^i \zeta \tag{4.7}$$

$$v_e = H_2^i \zeta \tag{4.8}$$

where $\zeta = [x \quad i_s \quad v_g]^T$, A_m^i, B_{sm}^i, B_{rm}^i, C_m^i and H_m^i are defined in Appendix C. The superscript "i" denotes the interconnected system of the filter and the regulator.

Using the state-space averaging technique outlined earlier, one can approximate the switched system by the large-signal continuous-time system

$$\dot{\bar{\zeta}} = (A_1^i d + A_2^i d')\bar{\zeta} + (B_{s1}^i d + B_{s2}^i d')\bar{v}_s + (B_{r1}^i d + B_{r2}^i d')V_{ref} \tag{4.9}$$

$$\bar{v}_o = (C_1^i d + C_2^i d')\bar{\zeta} \tag{4.10}$$

$$\bar{v}_e = (H_1^i d + H_2^i d')\bar{\zeta} \tag{4.11}$$

where $\bar{\zeta}$ represents the average states of the interconnected system. This model will be used to study the filter-regulator interaction on the slow scale. Note that, for the averaged model, the switching condition will stay as before

$$d = \frac{1}{V_m}\bar{v}_e \tag{4.12}$$

The exact discrete-time model of the interconnected system can be obtained as before

$$\begin{aligned}
\zeta(n+1) &= e^{A_2^i d'(n)T} e^{A_1^i d(n)T} \zeta(n) \qquad (4.13)\\
&+ \left[e^{A_2^i d'(n)T}\left(e^{A_1^i d(n)T} - I\right)(A_1^i)^{-1}B_{s1}^i + \left(e^{A_2^i d'(n)T} - I\right)(A_2^i)^{-1}B_{s2}^i\right] v_s\\
&+ \left[e^{A_2^i d'(n)T}\left(e^{A_1^i d(n)T} - I\right)(A_1^i)^{-1}B_{r1}^i + \left(e^{A_2^i d'(n)T} - I\right)(A_2^i)^{-1}B_{r2}^i\right] V_{ref}\\
v_o(n+1) &= C_2^i \zeta(n+1) \qquad (4.14)
\end{aligned}$$

The map (4.13) will be used to study the total behavior of the system: slow and fast. The switching condition is again the same as before

$$v_e(d(n)T) = v_{ramp}(d(n)T) \tag{4.15}$$

Clearly, Eqs. (4.9)-(4.12) define the complete interconnected filter-regulator system as a nonlinear continuous-time system. On the other hand, Eqs. (4.13)-(4.15) define the filter-regulator system as a nonlinear discrete-time system. We shall use both models to predict the bifurcations of the system, with the source voltage as the bifurcation parameter.

4.2 Stability Analysis

To facilitate analytical evaluation of the effect of the input filter on the regulator operation, we use the previous design of the buck converter. For the controller design, we use the PID controller with the gain of 96 dB. Note that the operation of this regulator without the input filter was found to be stable for a DC source voltage varying from 20V to 40V. In the classical theory of filter-regulator interactions, the small-signal stability of a switching converter with an input filter can be found by comparing the output impedance of the filter to the input impedance of the switching regulator. For a given load resistance, the controller adjusts the duty ratio to maintain a constant output voltage, hence a constant output power. Thus, if the input voltage increases, the input current must decrease to yield a constant input power. Consequently, the switching regulator exhibits a negative input impedance. The input impudence of the three types of converters can be found in detail in (Middlebrook, 1978). In general, for low frequencies, the input impudence of the buck regulator is dominated by the load resistance R and is given by

$$Z_i(low) = -\frac{R + R_L}{D^2} \tag{4.16}$$

where D is the nominal duty ratio of the buck converter. At the resonant frequency of the output filter $\omega_0 = 1/\sqrt{LC}$, the input impedance is at its minimum and is given by

$$Z_i(min) = -\frac{R_L}{D^2} \tag{4.17}$$

Above the resonant frequency, the input impedance increases inductively as

$$Z_i(high) = -\frac{sL}{D^2} \tag{4.18}$$

The output impedance of the second-order input EMI filter is

$$Z_s = \frac{sL_s + R_s}{C_s L_s s^2 + R_s C_s s + 1} \tag{4.19}$$

The negative input impedance of the switching regulator in conjunction with the input filter can, under certain conditions, constitute an oscillator with a negative resistance, thereby causing system instability. The output impedance of the input filter is a small positive resistance at DC and low frequencies, but, in the neighborhood of the filter resonant frequency, its magnitude may be many times the associated ohmic resistances. Hence, if the magnitude of Z_s increases sufficiently so that the net circuit resistance becomes negative, oscillations will occur on the slow scale (average behavior). Therefore, if the maximum output impedance of the input filter $|Z_s|(max)$ is less than the magnitude of the input impedance of the switching converter $|Z_i|$ for all frequencies, the system is guaranteed to be stable. Note that violation of this condition does not necessarily lead to instability. Further study using the Nyquist stability criterion should be used, where, in this case, a minor loop gain is defined as

$$T_m = \frac{Z_s}{Z_i} \tag{4.20}$$

Nyquist stability criterion is applied to T_m to determine the stability of the interconnected system. In Fig. 4.2, the magnitude of the input impedance of the regulator $|Z_i|$ is shown for different regulator input voltages. The filter output impedance $|Z_s|$ is also shown. The parameters used for this filter are $L_s = 1000\mu$H, $C_s = 47\mu$F, and $R_s = 1\Omega$. As one can clearly see, $|Z_i|$ is always greater than $|Z_s|$ for the whole frequency and source voltage ranges. Consequently, the system stability is guaranteed and no interactions are predicted on the

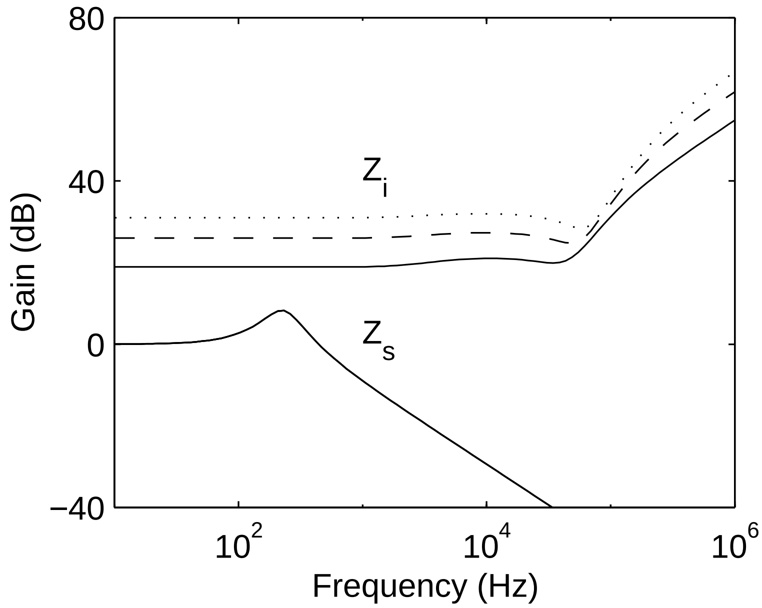

Figure 4.2: Regulator input impedance Z_i and the output impedance of the first input filter Z_s for different values of source voltage. (——) $v_s = 20$V, (– – –) $v_s = 30$V, and (· · · · ·) $v_s = 40$V.

slow scale. This design is considered to be a good design based on the guidelines presented in the filter-regulator literature. However, in Fig. 4.3, for the same regulator design and a different filter design with the capacitance of the filter changed to 470μF, interaction is predicted to occur due to the encirclement of the minor loop gain of -1. Note that, in this case, the denominator of the minor loop gain has two complex conjugate roots in the right-half of the complex plane. Hence, the system will oscillate below an input voltage of approximately 32V. The system in this case is said to be poorly designed.

Although the above frequency analysis allows the determination of the linear stability of the

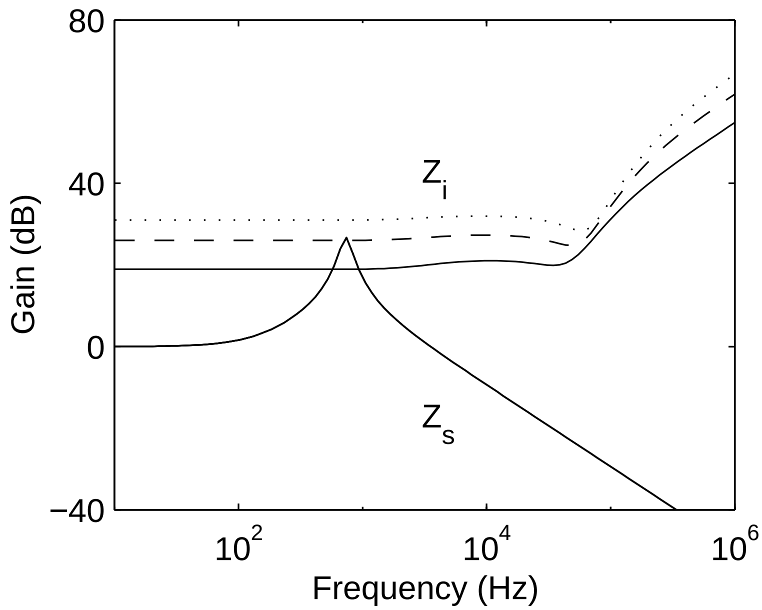

Figure 4.3: Regulator input impedance Z_i and the output impedance of the second input filter Z_s for different values of source voltage. (——) $v_s = 20$V, (− − −) $v_s = 30$V, and (· · · · ·) $v_s = 40$V.

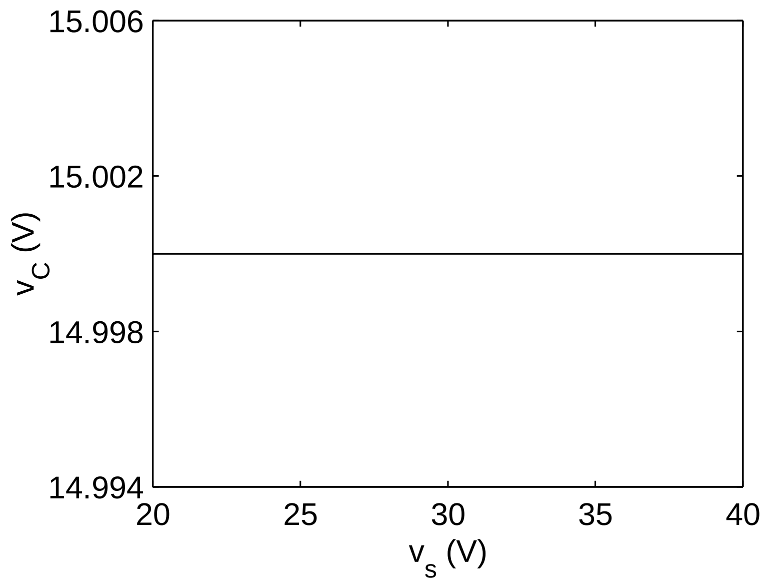

Figure 4.4: Equilibrium solution of the large-signal averaged model with the first filter used. (——) stable solution and (– – –) unstable solution.

system on the slow scale (average behavior), it does not predict the nonlinear stability. To demonstrate this, we use the large-signal model of the interconnected system (4.9)-(4.12). The equilibrium solutions can be easily obtained by setting $\dot{\zeta}$ equal to zero and solving the resulting nonlinear system. The stability of the equilibria can be found by calculating the eigenvalues of the Jacobian matrix J. As shown in Fig. 4.4, the equilibrium solutions of the averaged system using the first filter design are stable for the whole operating range, as expected from the previous small-signal analysis. Using the second filter, we would expect to see the equilibrium solutions losing stability below a source voltage of 32V, and indeed, as shown in Fig. 4.5, instability occurs as two eigenvalues enter the right-half of the complex plane when the source voltage is decreased, indicating a Hopf bifurcation.

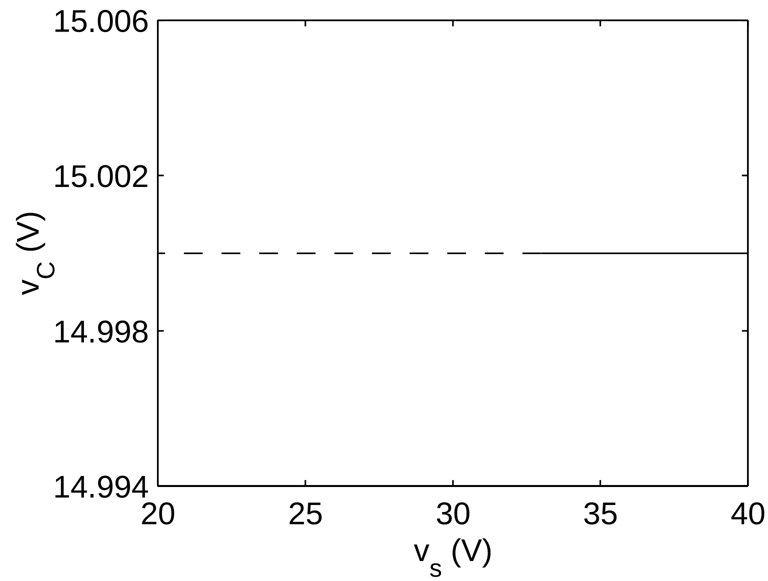

Figure 4.5: Equilibrium solutions of the large-signal averaged model with the second filter used. (——) stable solution and (– – –) unstable solution.

Using the method of multiple scales, we simplify the large-signal model near the Hopf bifurcation into the two-dimensional system of equations called the normal form (Nayfeh and Balachandran, 1995)

$$\dot{a} = \alpha_1(v_s - v_{s0})a + \alpha_2 a^3 \tag{4.21}$$

$$a\dot{\theta} = \alpha_3(v_s - v_{s0})a + \alpha_4 a^4 \tag{4.22}$$

where a is a measure of the amplitude of the created limit cycles. v_{s0} is the value of the source voltage at the Hopf bifurcation point. The bifurcation is generic if α_1 is different from zero. $\alpha_2 < 0$ indicates a subcritical bifurcation, and $\alpha_2 > 0$ indicates a supercritical bifurcation. A *Mathematica* code written by Nayfeh and Chin (1996) was used to calculate the coefficients in the normal form of the Hopf bifurcation. For the Hopf bifurcation at $v_s = 32V$, $\alpha_1 = -33.46$ and $\alpha_2 = 0.37$, which indicates that the bifurcation is generic and subcritical, hence, unstable limit cycles are born near the bifurcation point. Using a continuation scheme, we numerically determine the limit cycles as v_s is varied and obtain the bifurcation diagram shown in Fig. 4.6. As clearly shown in Fig. 4.6, there are large stable periodic solutions coexisting with the nominal stable equilibrium solutions. The region (32V-34V) is not a safe operation region and should be avoided. The small-signal analysis does not predict this solution. Clearly, the stability limit predicted by the linear analysis is below that predicted by the nonlinear large-signal analysis. Besides the Hopf bifurcation, the system response undergoes a cyclic-fold bifurcation at v_s = 34V, where two branches of unstable and stable limit cycles coalesce and obliterate each other as v_s is increased beyond 34V.

The averaged methods (frequency and time) can only give stability predictions of the slow

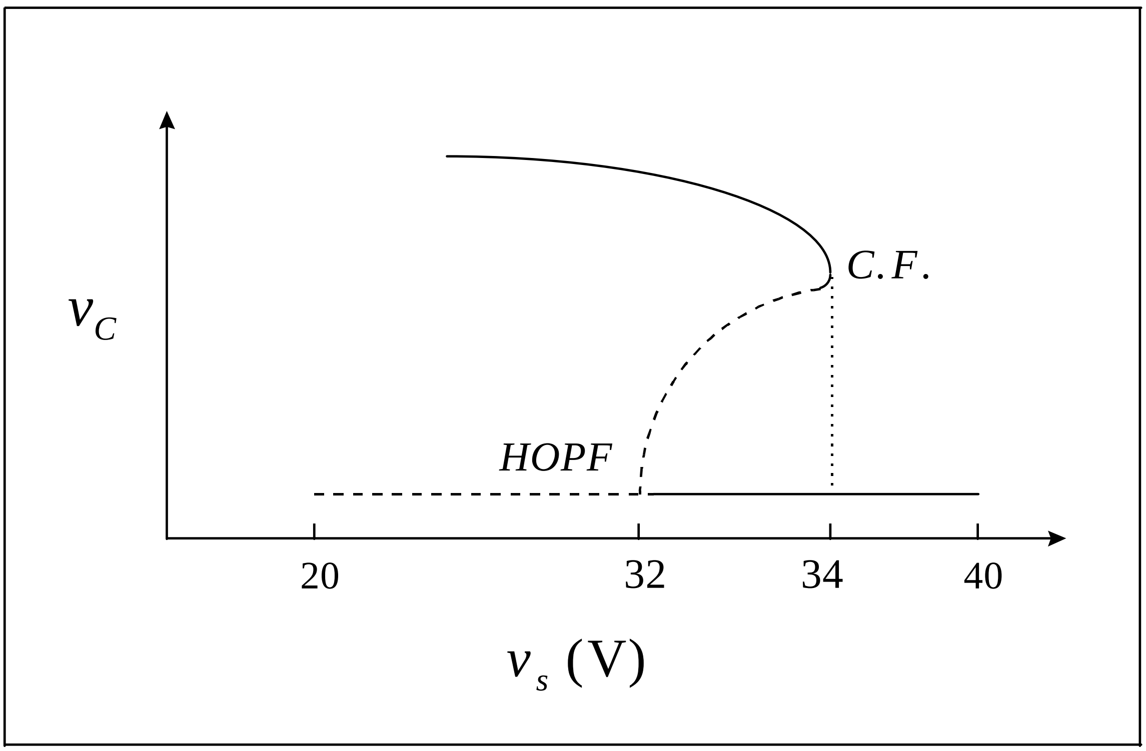

Figure 4.6: A bifurcation diagram of dynamic solutions of the filter-regulator system with the second filter used. HOPF = Hopf bifurcation and C.F. = Cyclic Fold bifurcation.

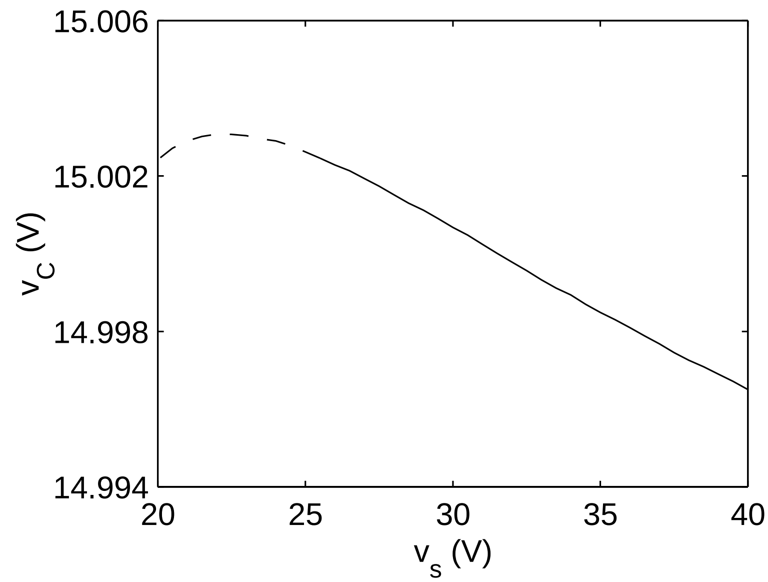

Figure 4.7: Period-one equilibrium solutions with the first filter used. (——) stable solution and (– – –) unstable solution.

or average behavior of the system. To investigate the fast dynamics and the stability of the total behavior of the system, we use the exact nonlinear model (4.13)-(4.15) developed earlier. In Fig. 4.7, we show the period-one equilibrium solution of the system using the first filter design. It loses stability below an input voltage of 25V. Because the slow dynamics have been shown to be stable, this instability is expected to be associated with the fast dynamics. Indeed looking at the movement of the eigenvalues, we can see that one of the eigenvalues is exiting the unit circle through -1, as shown in Fig. 4.8, which is the case for period-doubling bifurcation.

The period-one equilibrium solutions of the stand-alone system (i.e., without the input filter) are stable for the whole source voltage range, as shown in Fig. 4.9. Hence the input filter

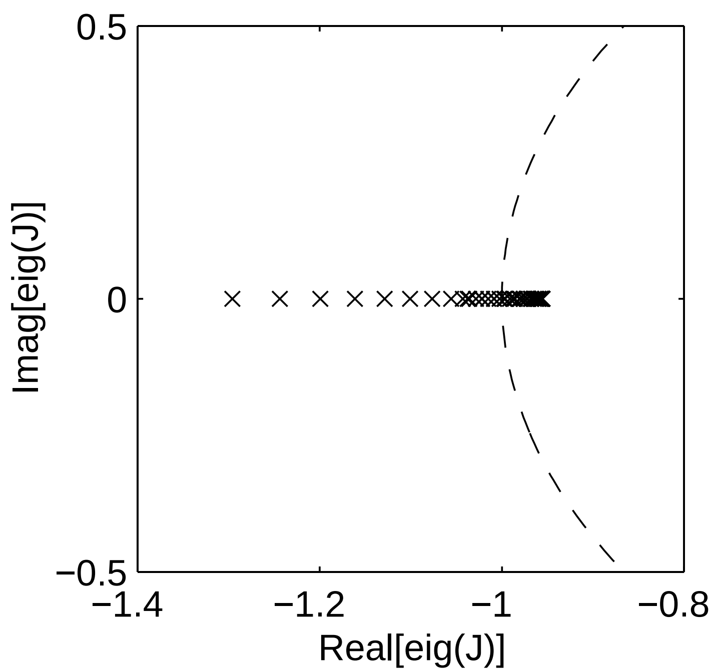

Figure 4.8: Locus of the eigenvalues as the source voltage is varied for the filter-regulator system with the first filter used.

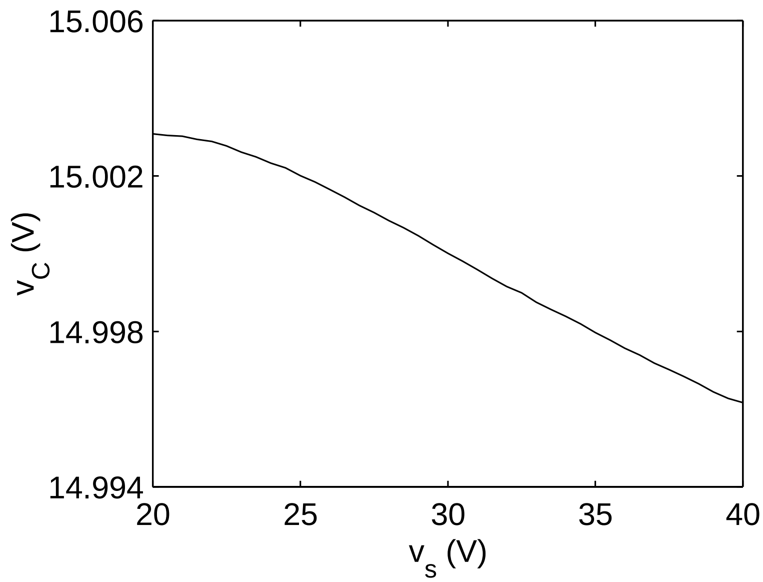

Figure 4.9: Period-one equilibrium solutions without the input filter.

has destabilized the fast dynamics of the regulator, although the filter-regulator system was designed using the guidelines outlined by Middlebrook (1976). In other words, although the stand-alone regulator is stable for a certain input voltage range, it loses stability by the addition of the input filter. Using the second filter design, as expected, the equilibrium solution loses stability below 32V. Two complex-conjugate eigenvalues exit the unit circle away from the real axis, confirming the instability of the slow dynamics. See Figs. 4.10 and 4.11.

In summary, the addition of the input filter destabilized the regulator operation on both scales: slow and fast. On the slow scale, the instability is in the form of a subcritical bifurcation. On the fast scale, the instability takes the form of a period-doubling route to chaos. In both cases, nonlinear analysis is needed to predict and study these bifurcations.

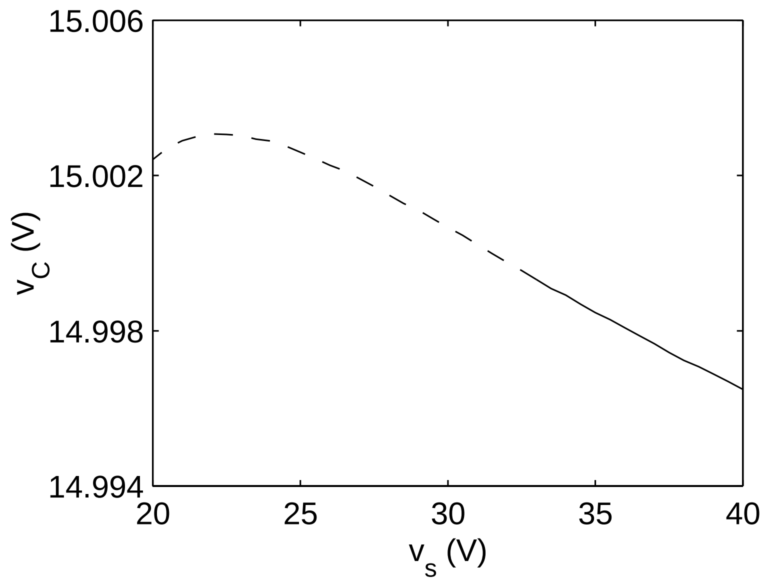

Figure 4.10: Period-one equilibrium solutions with the second filter used. (——) stable solution and (– – –) unstable solution.

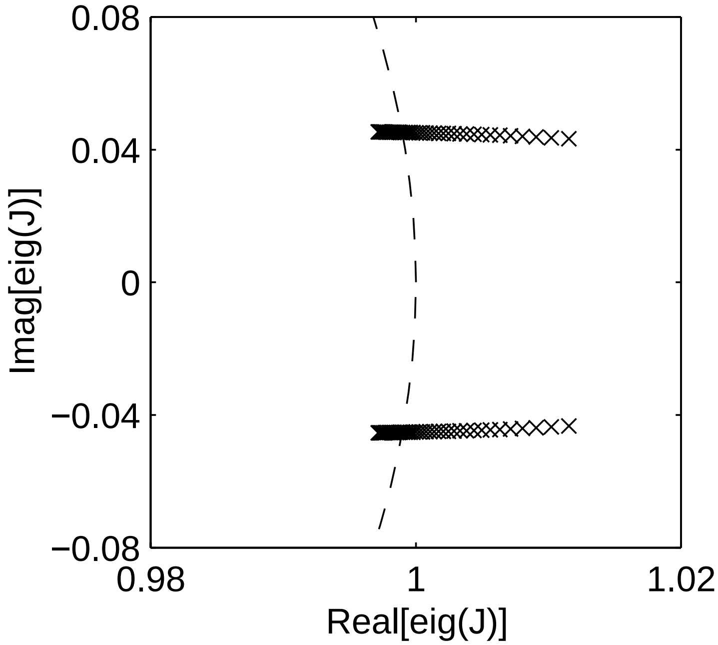

Figure 4.11: Locus of the eigenvalues of the filter-regulator system with the second filter used.

Chapter 5

Conclusions

A nonlinear model was derived for DC-DC regulators. It consists of a discrete difference equation in addition to a switching constraint. Unlike approximate averaged or sampled-data models, this model enables the designer to investigate the behavior of the system in all regions of operation: stable and unstable. Equilibrium solutions were calculated and their stability was investigated. Then, bifurcation diagrams were generated to study the total behavior of the system as one of its parameters varies. Whereas the averaged model is capable of predicting the instabilities resulting from slow disturbances, it is incapable of predicting the instabilities resulting from the fast dynamics, such as subharmonics and chaos. On the other hand, using the exact nonlinear model, one can predict the instabilities resulting from slow and fast disturbances. The exact model was used to study the stability of DC-DC regulators with different compensation schemes. Comparing the dynamic behaviors of these systems, we found that instability exists in practical regulators even when the conventional design guidelines were followed.

It was also shown that the average or slow dynamics of DC-DC switching regulators can be destabilized by the addition of an EMI input filter. Existing analysis techniques can only predict the local slow-scale stability. With the help of nonlinear analysis, nonlinear boundaries were identified using the large-signal averaged model. Complete interaction on the fast scale was also studied. Using the switching model of the regulator, we carried out a stability analysis on the fast scale and found out that destabilization occurs due to the interaction, which was confirmed through eigenvalue analysis.

Bibliography

Brockett, R. W and Wood, J. R., 1984, "Understanding power converter chaotic behavior mechanisms in protective and abnormal modes," *Proceedings of the Powercon*, Vol. 11, No. 4, 1-15.

Brown, A. R. and Middlebrook, R. D., 1981, "Sampled-data modeling of switching regulators," *Power Electronics Specialists Conference*, 349-369.

Capel, A., Ferrante, J. G., and Prajoux, R., 1975, "State-variable stability of multi-loop PWM controlled DC/DC regulators in light and heavy mode," *Power Electronics Specialists Conference*, 91-103.

Chan, W. C. Y. and Tse, C. K., 1996a, "Studies of routes to chaos for current-programmed DC/DC converters," *Power Electronics Specialists Conference*, 789-795.

Chan, W. C. Y. and Tse, C. K., 1996b, "Bifurcation in bifurcation from a current-programmed DC/DC boost converter," *IEEE International Symposium on Circuits and Systems*, 249-252.

Cuk, S. and Middlebrook, R. D., 1977, "A general unified approach to modeling switching DC-to-DC converters in discontinuous conduction mode," *Power Electronics Specialists Conference* , 36-57.

Deane, J. H. B. and Hamill, D. C., 1990, "Analysis, simulation and experimental study of chaos in the buck converter," *Power Electronics Specialists Conference*, 491-498.

Deane, J. H. B., 1992, "Chaos in a current-mode controlled boost DC-DC converter," *IEEE Transactions on Circuits and Systems I: Fundamental Theory and Applications*, Vol. 39, No. 8, 680-683.

Fossas, E. and Olivar, G., 1996, "Study of chaos in the buck converter," *IEEE Transactions on Circuits and Systems I: Fundamental Theory and Applications*, Vol. 43, No.1, 13-25.

Hamill, D. C. and Jefferies, D. J., 1988, "Subharmonics and chaos in a controlled switched-mode power converter," *IEEE Transactions on Circuits and Systems*, Vol. 35, No. 8, 1059-1061.

Hamill, D. C., Deane, J. H. B., and Jefferies, D. J., 1992, "Modeling of chaotic DC-DC converters by iterated nonlinear mappings," *IEEE Transactions on Power Electronics*, Vol. 7, No. 1, 25-36.

Jefferies, D. J., Deane, J. H. B., and Johnstone, G. G., 1989, "An introduction to chaos," *Electronics & Communication Engineering Journal*, Vol. 1, No. 3, 115-123.

Kassakian, J. G., Schlecht, M. F., and Verghese, G. C., 1991, *Principles of Power Electronics*, Addison-Wesely, Reading, Massachusetts.

Krein, P. T. and Bass, R. M., 1989, "Multiple limit cycle phenomena in switching power converters," *IEEE Applied Power and Electronics Conference and Exposition*, 143-148.

Krein, P. T. and Bass, R. M., 1990, "Types of instability encountered in simple power electronic circuits: unboundedness, chattering, and chaos," *Fifth Annual Applied Power Electronics Conference and Exposition*, 191-194.

Lee, F. C. Y., Iwens, R. P. and Yu, Y., 1979, "Generalized Computer-aided Discrete Time-Domain Modeling and Analysis of DC-DC Converters," *IEEE Transactions on Industrial Electronics and Control Instrumentation*, Vol. 26, No. 2, 58-69

Lee, F. C., and Yu, Y., 1979, 'Input-Filter Design for Switching Regulators,' *IEEE Transactions on Aerospace and Electronics Systems*, Vol. 15, No. 5, 627-634.

Marrero, J. L. R., Font, J. M., and Verghese, G. C., 1996, "Analysis of the chaotic regime for DC-DC converters under current-mode control," *Power Electronics Specialists Conference*, 1477-1483.

Middlebrook, R. D., 1976, "Input Filter Considerations in Design and Applications of Switching Regulators," *Proceedings of the IEEE on Industry Applications*, 91-107.

Middlebrook, R. D., 1978, "Design techniques for preventing input-filter oscillations in switched-mode regulators," *Proceedings of Powercon 5*, p.A3/1-16.

Middlebrook, R. D. and Cuk, S., 1977, "A general unified approach to modelling switching-converter power stages," *Power Electronics Specialists Conference*, 521-550.

Nayfeh, A. H. and Balachandran B., 1995, *Applied Nonlinear Dynamics*, John Wiley, New York.

Prajoux, R., Marpinard, J. C., and Jalade, J., 1976, "Establishing mathematical models of power regulators with pulse width modulation (PWM)," *ESA Scientific and technical Review*, Vol. 2, No. 1, 25-42.

Ridley, R. B., 1991, "A new continuous-time model for current-mode control," *IEEE Transactions on Power Electronics*, Vol. 6, No. 2, 271-280.

Shortt, D. J. and Lee, F. C., 1983, "Improved switching converter model using discrete and averaging techniques," *IEEE Transactions on Aerospace and Electronic Systems*, Vol. 19, No. 2, 190-202.

Tse, C. K. and Adams, K.M., 1990, "Qualitative analysis and control of a DC-to-DC boost converter operating in discontinuous mode," *IEEE Transactions on Power Electronics*, Vol. 5, No. 3, 323-330.

Tse, C. K. and Adams, K. M., 1991, "A nonlinear large-signal feedforward-feedback control for two-state DC-DC converters," *Power Electronics Specialists Conference*, 722-729.

Tse, C. K., 1994a, "Flip bifurcation and chaos in three-state boost switching regulators," *IEEE Transactions on Circuits and Systems I: Fundamental Theory and Applications*, Vol. 41, No. 1, 16-23.

Tse, C. K., 1994b, “Chaos from a buck switching regulator operating in discontinuous mode,” *International Journal of Circuit Theory and Applications*, Vol. 22, No. 4, 263-278.

Vorperian, V., 1990a, “Simplified analysis of PWM converters using model of PWM switch. Part I: Continuous conduction mode,” *IEEE Transactions on Aerospace and Electronic Systems*, Vol. 26, No. 3, 490-496.

Vorperian, V., 1990b, “Simplified analysis of PWM converters using model of PWM switch. Part II: Discontinuous conduction mode,” *IEEE Transactions on Aerospace and Electronic Systems*, Vol. 26, No. 3, 497-505.

Wester, G. W. and Middlebrook, R. D., 1972, “Low-frequency characterization of switched DC-DC converters,” IEEE Transactions on Aerospace and Electronic Systems, Vol. 9, No. 3, 376-85.

Wood, J. R., 1989, “Chaos: a real phenomenon in power electronics,” *Fourth Annual IEEE Applied Power and Electronics Conference and Exposition*, 115-124.

Yu, Y. and Biess, J. J., 1971, “Some Design Aspects Concerning Input Filters for DC-DC Converters,” *Power Conditioning Specialists Conference*, 66-76.

Zafrany, I. and Ben-Yaakov, S., 1995, “A chaos model of subharmonic oscillations in current mode PWM boost converters,” *Power Electronics Specialists Conference*, 1111-1117.

Appendix A

Open-Loop System

For a buck converter:

$$A_1^o = \begin{bmatrix} -\frac{1}{L}(R_L + \frac{RR_C}{R+R_C}) - \frac{R}{(R+R_C)L} & \\ \frac{R}{(R+R_C)C} & -\frac{1}{(R+R_C)C} \end{bmatrix}, \quad B_1^o = \begin{bmatrix} \frac{1}{L} \\ 0 \end{bmatrix}$$

$$A_2^o = \begin{bmatrix} -\frac{1}{L}(R_L + \frac{RR_C}{R+R_C}) & -\frac{R}{(R+R_C)L} \\ \frac{R}{(R+R_C)C} & -\frac{1}{(R+R_C)C} \end{bmatrix}, \qquad B_2^o = \begin{bmatrix} 0 \\ 0 \end{bmatrix}$$

$$C_1^o = \begin{bmatrix} \frac{RR_c}{R+R_C} & \frac{R}{R+R_C} \end{bmatrix}, \qquad C_2^o = \begin{bmatrix} \frac{RR_c}{R+R_C} & \frac{R}{R+R_C} \end{bmatrix}$$

For a boost converter:

$$A_1^o = \begin{bmatrix} -\frac{R_L}{L} & 0 \\ 0 & -\frac{1}{(R+R_C)C} \end{bmatrix}, \qquad B_1^o = \begin{bmatrix} \frac{1}{L} \\ 0 \end{bmatrix}$$

$$A_2^o = \begin{bmatrix} -\frac{1}{L}(R_L + \frac{RR_C}{R+R_C}) & -\frac{R}{(R+R_C)L} \\ \frac{R}{(R+R_C)C} & -\frac{1}{(R+R_C)C} \end{bmatrix}, \quad B_2^o = \begin{bmatrix} \frac{1}{L} \\ 0 \end{bmatrix}$$

$$C_1^o = \begin{bmatrix} 0 & \frac{R}{R+R_C} \end{bmatrix}, \qquad C_2^o = \begin{bmatrix} \frac{RR_c}{R+R_C} & \frac{R}{R+R_C} \end{bmatrix}$$

For a buck-boost converter:

$$A_1^o = \begin{bmatrix} -\frac{R_L}{L} & 0 \\ 0 & -\frac{1}{(R+R_C)C} \end{bmatrix}, \qquad B_1^o = \begin{bmatrix} \frac{1}{L} \\ 0 \end{bmatrix}$$

$$A_2^o = \begin{bmatrix} -\frac{1}{L}(R_L + \frac{RR_C}{R+R_C}) & -\frac{R}{(R+R_C)L} \\ \frac{R}{(R+R_C)C} & -\frac{1}{(R+R_C)C} \end{bmatrix}, \quad B_2^o = \begin{bmatrix} 0 \\ 0 \end{bmatrix}$$

$$C_1^o = \begin{bmatrix} 0 & \frac{R}{R+R_C} \end{bmatrix}, \qquad C_2^o = \begin{bmatrix} \frac{RR_c}{R+R_C} & \frac{R}{R+R_C} \end{bmatrix}$$

Appendix B

Closed-Loop System

$$A_1^c = \begin{bmatrix} A_1^c & 0 \\ GC_1^o & F \end{bmatrix}, \quad B_{g1}^c = \begin{bmatrix} B_1^o \\ 0 \end{bmatrix}, \quad B_{r1}^c = \begin{bmatrix} 0 \\ Q \end{bmatrix}$$

$$A_2^c = \begin{bmatrix} A_2^c & 0 \\ GC_2^o & F \end{bmatrix}, \quad B_{g2}^c = \begin{bmatrix} B_2^o \\ 0 \end{bmatrix}, \quad B_{r2}^c = \begin{bmatrix} 0 \\ Q \end{bmatrix}$$

$$C_1^c = \begin{bmatrix} C_1^o & 0 \end{bmatrix}, \quad C_2^c = \begin{bmatrix} C_2^o & 0 \end{bmatrix}$$

$$H_1^c = \begin{bmatrix} 0 & H \end{bmatrix}, \quad H_2^c = \begin{bmatrix} 0 & H \end{bmatrix}$$

Appendix C

Filter-Regulator System

$$
A_1^i = \begin{bmatrix} A_1^c & & 0 & B_{g1}^c \\ 0 & 0 & -\frac{R_s}{L_s} & -\frac{1}{L_s} \\ -\frac{a_1}{C_s} & 0 & \frac{1}{C_s} & 0 \end{bmatrix}, \quad B_{s1}^i = \begin{bmatrix} 0 \\ \frac{1}{L_s} \\ 0 \end{bmatrix}, \quad B_{r1}^i = \begin{bmatrix} B_{r1}^c \\ 0 \\ 0 \end{bmatrix}
$$

$$
A_2^i = \begin{bmatrix} A_2^c & & 0 & B_{g2}^c \\ 0 & 0 & -\frac{-R_s}{L_s} & -\frac{1}{L_s} \\ -\frac{a_2}{C_s} & 0 & \frac{1}{C_s} & 0 \end{bmatrix}, \quad B_{s2}^i = \begin{bmatrix} 0 \\ \frac{1}{L_S} \\ 0 \end{bmatrix}, \quad B_{r2}^i = \begin{bmatrix} B_{r2}^c \\ 0 \\ 0 \end{bmatrix}
$$

$a_1 = 1$ for the three types of converters, and

$a_2 = 0$ for a buck and a buck-boost converters, and 1 for a boost converter.

$$C_1^i = \left[\begin{array}{cc} C_1^c & 0 \end{array} \right], \quad C_2^i = \left[\begin{array}{cc} C_2^c & 0 \end{array} \right]$$

$$H_1^i = \left[\begin{array}{ccc} H_1^c & 0 & 0 \end{array} \right], \quad H_2^i = \left[\begin{array}{ccc} H_2^c & 0 & 0 \end{array} \right]$$

Vita

Mohammed Al-Fayyoumi was born on February 7, 1972 in Kuwait. He received his B.S. in Electrical Engineering from the Jordan University of Science and Technology, Irbid, Jordan in 1996. After that he joined Virginia Polytechnic Institute and State University to continue his higher education. He is currently a member of the Phi Kappa Phi honor society, and the Eta Kappa Nu honor society for electrical engineers. He is a student member of the IEEE.